Submitted to Astronomical Journal.

B-Star Rotational Velocities in h and χ Persei: A Probe of Initial Conditions During the Star-Formation Epoch?

Stephen E. Strom[1] and Sidney C. Wolff[1]

National Optical Astronomy Observatory, P.O. Box 26732, Tucson, AZ 85726

sstrom@noao.edu

and

David H. A. Dror[1]

Cornell University and National Optical Astronomy Observatory

ABSTRACT

Projected rotational velocities (*v sin i*) have been measured for 216 B0–B9 stars in the rich, dense h and χ Persei double cluster and compared with the distribution of rotational velocities for a sample of field stars having comparable ages ($t \sim$ 12-15 Myr) and masses (M $\sim$ 4-15 $M\odot$). For stars that are relatively little evolved from their initial locations on the Zero Age Main Sequence (those with masses M $\sim$ 4-5 $M\odot$), the mean *v sin i* measured for the h and χ Per sample is slightly more than 2 times larger than the mean determined for field stars of comparable mass, and the cluster and field *v sin i* distributions differ with a high degree of significance. For somewhat more evolved stars with masses in the range 5-9 $M\odot$, the mean *v sin i* in h and χ Per is 1.5 times that of the field; the *v sin i* distributions differ as well, but with a lower degree of statistical significance. For stars that have evolved significantly from the ZAMS and are approaching the hydrogen exhaustion phase (those with masses in the range 9-15 $M\odot$), the cluster and field star means and distributions are only slightly different. We argue that both the higher rotation rates and the pattern of rotation speeds as a function of mass that differentiate main sequence B stars in h and χ Per

[1]NOAO is operated by the Association of Universities for Research in Astronomy (AURA), Inc. under cooperative agreement with the National Science Foundation.

from their field analogs were likely imprinted during the star formation process rather than a result of angular momentum evolution over the 12-15 Myr cluster lifetime. We speculate that these differences may reflect the effects of the higher accretion rates that theory suggests are characteristic of regions that give birth to dense clusters, namely: (a) higher initial rotation speeds; (b) higher initial radii along the stellar birthline, resulting in greater spinup between the birthline and the ZAMS; and (c) a more pronounced maximum in the birthline radius-mass relationship that results in differentially greater spinup for stars that become mid- to late- B stars on the ZAMS.

Subject headings: stars: rotation—stars: formation—open clusters and associations: individual(h and χ Persei)

1. Introduction

Much of our current understanding of how stars form derives from the study of nearby star-forming regions such Taurus-Auriga, Ophiuchus, and Chamaeleon. These regions are populated by ~ 100 young stars having typical masses $M < 1 M\odot$ contained within irregular molecular cloud complexes that span regions of size $\sim$ 3-10 pc. However, the demographics and morphologies of these complexes differ markedly from those thought to produce the majority of stars over the history of the universe: dense stellar clusters containing 10^4 to 10^6 stars having masses ranging from 100 to 0.1 $M\odot$ formed within regions no more than $\sim$ 1pc in size. Do the dramatic differences in stellar density between these regions influence measurable properties of individual stars and the statistical properties (e.g. the initial mass function) of the emerging stellar populations? If so, what are the key physical causes? Answering these questions represents an essential first step toward developing a predictive theory of star formation of sufficient power to inform our understanding of how the mix of high and low mass stars populating galaxies today came to be, and as a consequence how the observed relative abundances of heavy elements were established.

The importance and timeliness of these questions have stimulated several recent theoretical studies aimed at predicting initial protostellar conditions in dense star-forming complexes (e.g. McKee & Tan 2003), and their relationship to emergent stellar mass functions (e.g. Elmegreen & Shadmehri 2003). Dense stellar clusters form in regions of very high gas surface density characterized as well by close packing of protostars. The turbulent velocity of the gas in these regions is likely to be high, leading to (1) protostars of high initial density; (2) rapid protostellar collapse times; and (3) as a consequence, high time-averaged accretion rates. The latter may be conducive to the formation of very high mass stars, since the dy-

namical pressure of accreting material can be high enough to overcome radiation pressure from the forming massive stars (McKee & Tan 2003). The combination of protostellar cores characterized by higher turbulent speeds and higher mass accretion rates, combined with collisions between closely packed cores, may in turn produce a 'top-heavy' IMF (Elmegreen & Shadmehri 2003).

These theoretical studies thus suggest: (1) higher time-averaged accretion rates; and (2) an initial mass function biased toward higher mass stars in high density stellar clusters. In principle, accretion rates characteristic of different star-forming regions can be diagnosed from the location of the stellar birthline (e.g. Stahler 1988) as determined from spectroscopic and photometric observations of precision sufficient to locate pre-main sequence stars spanning a range of masses in the HR diagram, provided that the target regions are young and accurate age estimates are available. Quantifying initial mass functions requires similar observations.

To date, it has not been possible to determine either birthline locations or IMFs spanning the full range of stellar masses primarily because the best and closest examples of high density clusters (e.g. Arches at the Galactic Center, Stolte et al. 2002; R 136 in the Magellanic Clouds, Massey & Hunter 1998; Sirianni et al. 2000) suffer from extreme crowding, which thus far has limited photometric and spectroscopic observations to main-sequence stars and a few pre-main-sequence stars with masses above $\sim 2M\odot$. Such stars are both bright enough to stand out relative to the stellar background and rare enough to avoid overlap with objects of comparable brightness. Next generation adaptive optics systems on current generation large telescopes have the potential to overcome the limitations of crowding and enable determination of stellar luminosities and effective temperatures for stars with masses as small as 0.1 $M\odot$, a level more than sufficient to confront theoretical predictions of IMF shape and birthline positions. However, until such systems become operational, other and less direct approaches must suffice. We explore here the possibility that the distribution of stellar rotational velocities can provide a surrogate indicator of the differences in initial conditions between low and high density star-forming regions. Our reasoning is as follows.

Current theory suggests that initial stellar angular momenta are established during the primary stellar accretion phase via locking of stellar angular velocity to the angular velocity of the circumstellar accretion disk at or near the radius, r(m), where the stellar magnetosphere links to the disk (e.g. Königl 1991; Shu et al. 1994). That radius is set by the balance between the dynamical pressure of accreting material and the magnetic pressure of the magnetic field rooted in the forming star. For a fixed stellar magnetic field strength, the higher the accretion rate through the disk, the smaller r(m), the higher the Keplerian rotation speed of the disk at r(m), and hence the higher the angular rotational speed of the

star. Hence, if accretion rates are higher in high density star-forming regions, the resulting stellar population would be expected to exhibit higher rotation speeds on average.

Supporting observational evidence in the literature is sparse, but highly suggestive. For example, Wolff, Edwards, & Preston (1982; hereafter WEP) note that the distribution of rotation speeds among B stars in the relatively dense Orion Nebula Cluster is significantly shifted toward higher values as compared to stars of similar type distributed among the much lower density regions of the Orion star-forming complex. Similarly, Slettebak (1968) argues that stellar rotation speeds among the luminous B giant stars located in the vicinity of the extremely dense h and χ Persei double cluster are $\sim$ 50% higher than their field counterparts. Moreover, he reports an unusually high number of rapidly rotating Be stars, possibly indicative of a higher fraction of rapidly rotating stars in h and χ Per. However, the Orion study includes only a modest sample of stars, while past discussions of h and χ Per rotation properties suffer from concerns regarding the similarity in age range among field and cluster cohorts combined with the possibility of evolutionary changes in stellar angular momenta. Confronting the hypothesis that stars born in dense clusters rotate more rapidly than their field counterparts requires sufficiently large samples of cluster and field stars spanning an identical range of ages.

The goal of this contribution is to effect a robust statistical comparison of the distribution of stellar rotational velocities for a sample of B0-B9 stars in h and χ Persei (typical stellar density of 10^4 pc^{-3}; Slesnick, Hillenbrand, & Massey, 2002, hereafter SHM) with those observed among field B stars of comparable age as determined from their location in the Strömgren (β, c$_0$) plane. This latter sample is almost certainly dominated by stars born in much lower density environments.

2. New Observations of B Stars in h and χ Persei

2.1. Spectroscopy

We report here new rotational velocity determinations of 216 stars in h and χ Per with estimated masses greater than 4 $M\odot$. These stars were chosen from the recent photometric and moderate resolution spectroscopic study of the double cluster by SHM. The basic data for the h and χ Per stars are listed in Table 1. Column 1 provides an identification from SHM; column 2 lists the Oosterhoff number; columns 3 and 4 list respectively the absolute visual magnitude M$_V$ and the log of the effective temperature derived by SHM; column 5 lists the spectral type if available; column 6 lists the mass derived by SHM; column 7 lists the derived value of *v sin i* (see below); column 8 lists a group assigned to the star on the basis

of its effective temperature(see below); in columns 9 and 10 we list the Strömgren indices c_0 and β, respectively, from the work of Capilla & Fabregat (2002) or Crawford, Glaspey, & Perry, (1970); and in column 11, we indicate whether the star is judged to be a spectroscopic binary with velocity amplitude K > 30 km/sec (see below). The HR diagram for these stars is shown in Figure 1. Also shown are evolutionary tracks from Schaller et al. (1992), with the M_{bol} from these tracks converted to M_V by using the relationship between bolometric correction and T_{eff} given by SHM.

For the purpose of later analysis, we divide the h and χ Per stars into three temperature groups, which are shown in Figure 1. We effected this division in order to examine separately the rotational properties of: (1) relatively unevolved stars, still located within 0.5 mag of the ZAMS; (2) stars located within 1 mag of the ZAMS; and (3) stars that have evolved significantly from the ZAMS. Comparison with the evolutionary tracks indicates that these three groups correspond to mass ranges of, approximately, 3.5-5 $M\odot$, 5-9 $M\odot$, and 9-15 $M\odot$. These groups are identified in Table 1 (column 8) as Group 1 (coolest and close to the ZAMS), Group 2 (middle range of temperature and slightly evolved from the ZAMS), and Group 3 (hottest and most evolved), respectively.

Spectra of the h and χ Per stars in our sample were obtained during three nights in September, 2002, with the Hydra multi-fiber spectrograph and the WIYN 3.5-meter telescope on Kitt Peak. The 316/63.4 echelle grating and a narrow-band order-separating filter were used in conjunction with the red bench camera to produce spectra with resolution ∼0.2 Å centered at a wavelength of λ4461 Å and spanning 120 Å. This wavelength region was selected in order to include the two strong features He I λ4471 and Mg II λ4481, which together provide the basis for determining accurate rotational velocities for stars in the desired spectral type range: B0-B9.

Eight separate fiber settings enabled observations of a total of 216 stars. Three settings were targeted at the brighter members of the cluster (8.5 < B < 12) and five at the fainter members (12 < B < 14.5). Exposure times were 30-60 minutes (divided among three exposures) for the bright sample and 90-120 minutes (divided among 3-4 exposures) for the faint sample. The series of three exposures for the bright stars was repeated either one or two nights later. Flat-field exposures and wavelength calibration observations derived from Th-Ar lamp spectra were obtained before or after each exposure.

The resulting spectra were extracted, cosmic-ray cleaned, combined and wavelength-calibrated using standard DOHYDRA IRAF reduction scripts. The resulting values of signal/noise ranged from 25 to 100 per resolution element for a typical target.

We also obtained spectra of 25 B1-B9 stars in the I Lac association; 18 of these stars, with

spectral types in the range B1-B3, have published projected rotational velocities spanning the range 20-365 km s^{-1} (Abt & Hunter 1962) and served as standards.

2.2. Derived Rotational Velocities

Rotational velocities for the hotter stars in our sample (stars in the two higher temperature groups shown in Figure 1) were determined (1) by establishing the relationship between the full-width at half maximum (FWHM) for He I and Mg II and projected rotational velocity (*v sin i*) for the I Lac rotational standard stars; and (2) using this relationship and the measured FWHM to establish *v sin i* for the unknowns (following Abt, Levato, & Grosso 2002, hereafter ALG). FWHM was determined from a Gaussian fit to the observed profiles. For the stars in these two groups, the He I line is substantially stronger than the Mg II line and was given twice the weight in deriving the average *v sin i* from the two lines. The relationships between FWHM and *v sin i* for the standard stars are shown in Figure 2, which demonstrates a good correlation between line width and *v sin i*.

Several stars in our h and χ Per sample that fall in our two higher temperature groups have also been observed by Gies & Huang (2003 and private communication). These authors derive values of *v sin i* by fitting three He I lines ($\lambda\lambda$4026, 4387, and 4471) with profiles derived from model atmospheres. Their computed profiles take limb and gravity darkening into account. Figure 3 shows a comparison between the values of *v sin i* derived by Gies & Huang and in the current study. The best fitting straight line is given by

$$vsini(Gies\&Huang) = 1.05(\pm 0.06)vsini(currentstudy) + 11(\pm 9)kms^{-1}. \quad (1)$$

Our results thus correlate well with the measurements of Gies & Huang but are systematically smaller by about 5%. Gies & Huang in turn state that their calibration agrees with the calibrations of Slettebak (1968; 1985) with a best fit slope of 0.999 and a zero point offset of 34 km s^{-1} in the sense that the Gies & Huang measurements are smaller than the Slettebak values. We have 13 stars in common with Slettebak and find that $v\ sin\ i(Slettebak) = 1.13v\ sin\ i(currentstudy) + 39kms^{-1}$, again indicating that our results are systematically slightly smaller. The Slettebak measurements were made from photographic plates with dispersions of 40 and 47 Å mm^{-1} and were insensitive to rotations less than about 50 km s^{-1}, which fact likely accounts for the zero-point offset.

To calibrate the rotational velocities for stars in the coolest temperature group, we made use of a previous set of Hydra observations of stars with low rotational velocities measured by ALG and having spectral types in the range B0-B8 (HR 1855, B0V, *v sin i* = 10 km/sec; HR 2222, B1V, *v sin i* = 0 km/sec; HR 153, B2IV, *v sin i* = 10 km/sec; HR

6042, B5V, *v sin i* = 30 km/sec; and HR 677, B8V, 25 km/sec). We artificially broadened these spectra by convolving the observed standard star spectra with a rotational-broadening profile corresponding to projected velocities of 50, 100, 150, 200, 300, 350, and 400 km/s. Over this entire spectral range, we find that the FWHMs of the calculated broadened line profiles are well correlated with rotation speed and that the slope and zero point of the relationships for λ4471 and λ4481 do not vary significantly with spectral type. Guided by this result, we chose to adopt the (*v sin i*, FWHM) relationships derived empirically for the two hotter groups for the cooler group as well. Because the He I and Mg II lines have similar equivalent widths for stars in the coolest group, the two lines were given equal weight in deriving *v sin i*.

Line widths become relatively insensitive to rotation once the rotation rate approaches the critical velocity owing to the effects of gravity darkening. Townsend, Owocki, & Howarth (2004) have constructed models of rapidly rotating B stars and find that for B0-B7 stars viewed equator-on and rotating at 95% of the critical velocity, the measured velocity will be up to 17% too low for measurements of Mg II 4481 and up to 33% too low for measurements of He I 4471 if gravity darkening is ignored. The effects are much smaller both for lower rotation rates and smaller angles of inclination. For stars in our sample, critical velocities range from about 400 to more than 500 km/sec. We find that N(*v sin i*), the distribution of apparent *v sin i*, decreases rapidly with increasing rotation above 250 km/sec. Only about 12% of the h and χ Per stars in the two lowest mass bins, and fewer than 5% of the field stars, appear to rotate faster than 300 km/sec (cf. Fig. 6). Hence, the fraction of our sample that might be strongly affected by gravity darkening is insignificant (< 10%).

The values of *v sin i* derived from the FWHMs are listed in column 7 of Table 1. Where more than one observation of a star is available, the quoted *v sin i* value represents an average of all determinations. The internal accuracy of our *v sin i* determinations can be assessed by comparing estimates derived from independent observations obtained on different nights. From such a comparison, we conclude that our reported *v sin i* values have an internal uncertainty of $\sim$10%. From the comparisons with the data of Gies & Huang and of Slettebak for h and χ Per, we have shown that the data transform to an externally calibrated system with a systematic uncertainty of about 5-10%.

2.3. Radial Velocities and the Search for Binaries

A number of studies (e.g. Abt & Hunter 1962; ALG) suggest possible correlations between binarity and observed rotational velocity. We have two methods for detecting binaries with our data set: 1) we can identify those spectra that have double lines; and 2) we can look

for stars with radial velocities that differ significantly from the cluster mean. For each star in our sample, we have derived a radial velocity from the observed line centroid wavelengths of the He I and Mg II lines.

The internal accuracy of the velocity determinations was judged by comparing the mean velocity derived from the He I and Mg II lines for three individual 1800 sec exposures that when summed constituted the 120 min observation of one of the faint fields. Because the pairs of exposures are separated by no more than 45 min, we expect any intrinsic radial velocity variations over this short time to be negligible compared to measurement errors. This comparison should give us a worst case estimate of the errors since the S/N of the observations of the faint stars is somewhat lower than for the bright stars and because (as we show in Section 4) the rotation rates of the fainter stars are somewhat higher and broader lines are harder to measure.

In Figure 4, we depict the cumulative distribution of velocity differences for one pair of exposures for the fainter stars in our sample. Note that about 85% of the stars have velocity differences that are less than 10 km/s. Only about 3% of the stars have velocity differences greater than 30 km/s, and the fact that a few stars have large errors is a consequence of the difficulty of measuring centroids of very broad lines.

This result provides the basis for compiling a list of candidate spectroscopic binaries. To be considered a candidate binary, the average velocity of a star on the summed exposures had to differ from the mean cluster velocity derived from the full sample of 216 stars by 30 km/sec. In addition, a few stars showed double lines. Column 11 of Table 1 indicates which stars are candidate spectroscopic binaries and the reason for their candidacy. For double-lined stars, the velocity listed is the difference in velocity of the two components. For single-lined stars, the table gives the difference between the stellar velocity and the cluster mean. The velocities marked with a colon are based on a single line. We have also compared the differences in velocity for the observations of bright stars taken on two different nights. Star 33 shows a change in velocity of 200 km/sec, which confirms its binary nature. Star 150 shows a velocity difference of 34 km/sec, just barely significant given our criteria. This star may also be a binary but has not been so designated in Table 1. We note finally, that our criterion for selecting candidate spectroscopic binaries could result in missing objects with velocity differences relative to the cluster mean close to 30 km/s in cases where the rotation speed of the primary exceeds 300 km/s. However, as noted previously, such rapidly rotating objects comprise less than 10 % of our field and cluster samples.

3. The Comparison Sample: Field B Stars

The B stars in h and χ Per are members of high stellar density bound systems. Isolated field B stars of ages comparable to that of h and χ Per ($\sim$12 Myr) are most likely drawn from stars born in much lower density environments: (a) stars formed initially in isolation or in small aggregates; or (b) stars whose peculiar motions have carried them several tens of parsecs away from their birthplaces in loose OB associations. The population of isolated field B stars may also contain a small number of stars born in dense environments but later ejected via gravitational encounters (runaway stars).

Extensive observations of rotational velocities for bright field B stars are available in the literature. The recent study by ALG provides a homogeneous database for a large (1092 stars) sample of field B stars listed in the Bright Star Catalog. Their observations were obtained with a CCD and have a resolution of 0.11 A or 7.1 km/sec. The rotational velocities quoted by ALG were calibrated against Slettebak et al. (1975) standards. Since Gies & Huang have shown that their data for h and χ Per are consistent with this system, and our measurements are about 5% smaller than the Gies & Huang values, a comparison between our h and χ Per data and the ALG data should be valid to within the externally-calibrated uncertainties of $\sim$5-10%. We note that while the ALG sample, drawn from the Bright Star Catalog, is dominated by isolated field stars, it contains as well a very modest number of stars located in relatively dense environments (e.g. the Orion Nebula Cluster). We have not attempted to exclude such stars from the sample, but note that including them will tend to reduce any differences between the distribution of rotational velocities between our h and χ Per and field samples.

The surface rotation rates of stars can be expected to change as stars evolve because of the changing moment of inertia of the star; transport of angular momentum within the star; and possible loss of angular momentum due to winds. Hence, in order to assess intrinsic differences in the distribution of rotation speeds among stars in h and χ Per and the field, it is essential that the field star sample include only objects having ages comparable to h and χ Per (12-15 Myr; see Figure 1 and Slesnick et al. 2002). To do this requires luminosity and effective temperature values of precision sufficient to enable age estimates. Because most stars in the ALG catalog lack parallaxes accurate enough to derive luminosities relative to the Zero Age Main Sequence (ZAMS) and thus stellar age, we have established their evolutionary state by using the Strömgren β and c_0 indices. These indices provide accurate estimates of surface gravity and effective temperature respectively, thus allowing evaluation of stellar ages: the youngest stars will have the highest surface gravities for fixed effective temperature (large β index at constant c_0), whereas more evolved stars will have lower surface gravities and thus smaller β indices.

In order to select field stars of ages comparable to those of the h and χ Per sample, we made use of the Strömgren β and c_1 indices listed by Hauck & Mermilliod (1998) for the ALG sample. For h and χ Per, values of β and c_1 are available from measurements reported by Crawford, Glaspey, & Perry (1970) and by Capilla & Fabregat (2002). Apropos photometry of the ALG sample, Hauck & Mermilliod (1998) have carefully transformed heterogeneous data from the literature to the Crawford system, noted discrepant values, and given them low weight. For h and χ Per, Capilla & Fabregat (2002) have used as standard stars objects in clusters measured by Crawford and collaborators, or objects measured by other investigators who made use of the same photometer-telescope combinations as Crawford. We thus believe that the Strömgren photometry for both the ALG field stars and the h and χ Per sample has been transformed carefully to the Crawford system and can thus be intercompared with confidence.

For the field stars, we used the relationship between intrinsic color (B-V) and spectral type (Drilling & Landolt 2000) to estimate the reddening and calculate the reddening-corrected Strömgren index, c_0. For those few stars for which values of B-V were not available from the Simbad database, we have assumed zero reddening. Given that the reddening $E(c_1)$ for the B stars for which we do have color information is typically 0.01-0.02 mag, and seldom exceeds 0.03 mag., any uncertainties in the reddening are unimportant for the analysis in this paper. The c_1 indices observed for the h and χ Per sample have been transformed to c_0 by assuming an average reddening of $E(b-y) = 0.4$ (i.e. $E(c_1) = 0.2E(b-y)$; see Capilla & Fabregat 2002). The relationships between β and M_V and c_0 and T_{eff} coupled with the group boundaries shown in Figure 1 were then used to establish boundaries between groups 1, 2 and 3 in the (β,c_0) plane. The subset of the ALG sample falling within these boundaries is plotted in Figure 5; the symbols indicate those stars in the ALG sample that correspond to Groups 1, 2 and 3. Also shown in this Figure are the location of the subset of stars in the h and χ Per sample for which published Strömgren photometry is available.

Table 2 lists the values of β and c_0 (or c_1 for the stars lacking B-V measurements; see above) for the field stars plotted in Figure 5 along with the values of $v\ sin\ i$ from ALG and the assignment of the star to one of the three temperature groups defined for the h and χ Per sample.

We note that the field stars in the ALG sample that fall within low (Group 1) and intermediate (Group 2) temperature groups comprise not only objects of luminosity class V but of luminosity classes III and even II (though the latter comprise $< 1\%$ of Groups 1 and 2). At first glance, this would appear surprising, given that stars in Groups 1 and 2 are expected to be little evolved from their initial location on the ZAMS and thus to have reported spectra consistent with assignment to luminosity class V. However, in the

temperature range spanned by these two groups, the actual difference in luminosity between class III and class V is quite modest. Quantitatively, the difference in the β,c_0 plane between the mean relationships for luminosity classes V and III is 0.04 mag in β, which corresponds to only 0.4 mag in absolute visual magnitude (Crawford, 1978). By comparison, the full range of β values at a given c_0 among late B stars nominally assigned to luminosity class V is almost 0.1 mag, thus resulting in significant overlap in β values with stars assigned to luminosity class III. Hence, the appearance of some stars classified as luminosity class III among the objects assigned to Groups 1 and 2 on the basis of their location in the (β,c_0) plane is in fact expected. That the range of β values is as large as 0.1 mag for a given spectral type and luminosity class, almost certainly reflects both the subjectivity inherent in any visual classification, as well as small errors introduced by assigning discrete spectral types as opposed to a continuously varying indicator of effective temperature, c_0.

Because (β,c_0) photometry provides finer resolution in both temperature and luminosity than MK classification, and because we have confidence that the ALG and h and χ Per sample have been transformed appropriately to the Crawford system, we believe that using the observed locations of the ALG and h and χ Per stars in the (β,c_0) plane provides the most reliable means of sorting each sample into identical temperature and age groups.

Could the use of photometric indices as opposed to spectroscopic sorting introduce any subtle selection biases? One concern is that rapid rotation may alter observed β and c_0 indices sufficiently to either exclude rapidly rotating stars from the sample, or to move them across the boundaries defining our three temperature groups. Empirical (Crawford, 1978) and theoretical (Collins & Sonneborn, 1977) studies suggest that changes in β and c_0, driven by temperature and gravity variations as a function of latitude among rotationally distorted stellar surfaces, are in practice significant only for stars having rotation speeds in excess of 250 km/sec. The most rapidly rotating stars among the cohort with rotation speeds in excess of 250 km/sec may exhibit Hβ emission, the presence of which could change measured β sufficiently to drive the star outside the bins used to define our groups. However, examination of the ALG sample suggest that only 8%, 6%, and 3% of stars in the temperature range spanned by groups 1, 2 and 3 respectively have rotation speeds higher than 250 km/sec. These percentages represent strong upper limits on the actual fraction of stars that would either be excluded from our sample completely, or moved from one group to another. Consequently, we believe that selection via location in the β,c_0 plane will not produce significant biases in the derived distributions of rotation speeds.

For the purpose of assessing whether the frequency of close binaries has an effect on the comparison of rotational velocities of the h and χ Per sample with stars in the field, we have searched the 9^{th} spectroscopic binary catalog (http://sb9.astro.ulb.ac.be) for orbital

parameters for stars in the ALG sample. In h and χ Per, we can detect binaries only if they differ from the cluster mean velocity by more than 30 km s^{-1} or if we see double lines. Therefore, in Table 3, we list those field stars that (a) meet our color criteria; (b) have orbital semi-amplitudes greater than 30 km s^{-1}; and/or (c) for which ALG reported seeing double lines. We recognize that the colors of spectroscopic binaries do not provide an accurate reflection of the temperature and surface gravity of the primary star, but we cannot make corrections for this effect for either h and χ Per or the field stars, and so will treat both samples identically.

4. Distribution of Rotational Velocities

In Figure 6, we plot the frequency distributions of rotational velocity N($v\ sin\ i$) for each of the three groups we have defined. All of the stars in our samples are included in the plots; these include the spectroscopic binary candidates identified in h and χ Per as well as the primaries of binaries in the field star sample. We have excluded the secondaries in the field star sample because in most cases we lack the temperature data needed to assign them to one of our three groups. In Figure 7, we plot the cumulative distributions for the $v\ sin\ i$ data shown in Figure 6. These figures suggest that the N($v\ sin\ i$) distribution for the h and χ Per group 1 stars (those that are little evolved from the ZAMS) is strikingly different from that of the field stars of similar mass and age. The distribution of $v\ sin\ i$ for the middle group of stars in h and χ Per also differs from that of the field stars in the same temperature range, but the difference is smaller. The distributions of $v\ sin\ i$ for evolved stars in the hottest group (group 3) exhibit only a small difference.

In all three temperature ranges, the sense of the difference is the same: while the number of rapid rotators ($v\ sin\ i$ > 250 km/sec) and the maximum rotation velocity measured are similar for both field and cluster stars, there is a marked deficiency of slow rotators ($v\ sin\ i$ < 100 km/sec) among the cluster stars. In order to assess the statistical significance of these differences, we calculated the corresponding KS probabilities that the distributions are drawn from the same distribution. These probabilities are $2\text{x}10^{-10}$, $9\text{x}10^{-6}$, and $9\text{x}10^{-3}$ for regions (1), (2), and (3) respectively.

Table 4 summarizes the average rotational velocities <$v\ sin\ i$> for the stars in h and χ Per and the field. If we consider all of the stars in the sample, including binaries, we find that for the unevolved stars in coolest temperature region (Group 1), the mean $v\ sin\ i$ in h and χ Per is twice that of their field counterparts and that the distributions are different with a high degree of significance. For stars in middle temperature range, the <$v\ sin\ i$> in h and χ Per is 1.56 times that of the field, and the distributions are different, with a lower

but still high degree of significance. For the evolved stars in region (3), <v *sin* i> in h and χ Per is only 1.25 times that of the field, and the distributions differ, but only marginally.

As a check on the robustness of our result, we computed mean values of vsini for the field stars using published spectral types and luminosity classes as opposed to Strömgren photometry. For the purposes of this test, the temperature boundaries for groups 1, 2 and 3 were defined to be B5-B9, B2.5-B5 and B0-B2 respectively. Stars with luminosity classes III-V were included. The resulting mean values are 112 km/s, 109 km/s, and 113 km/s respectively for groups 1,2 and 3. While these values differ by 15-20% from those listed in Table 4, our basic conclusions regarding the differences between the h and χ Per and field samples remain the same: the rotation speeds for groups 1 and 2 are significantly higher in h and χ Per as compared with the field, while for group 3, the rotation speeds between cluster and field are indistinguishable statistically.

The number of detectable spectroscopic binaries in h and χ Per is insufficient to enable comparison of the *distribution* of rotational velocities for the binaries among the three separate groups at a high level of statistical significance. Instead, we have calculated the mean rotational speeds, <v *sin* i>, for the binaries in each of the groups. We note that assignments to each of the groups are based on observed colors, which reflect the luminosity-weighted contributions from primary and secondary components. For all binaries the effective temperature of the primary assigned on the basis of color will thus be smaller than its true effective temperature.

The values of <v *sin* i> for the binaries with K > 30 km/sec and for the complementary samples excluding the binaries are compared in Table 4. For group 1, the field binaries have a <v *sin* i> value only 58% as large as <v *sin* i> for the field stars not in known binaries with K > 30 km/sec. For groups 1 and 2, the differences in <v *sin* i> between the binaries with K > 30 km/sec and the remaining stars in the same temperature range are not significant. Because only ∼10% of the stars show evidence of radial velocity variations greater than 30 km/sec, we conclude that the distributions of rotation speeds for h and χ Per and the field presented above are not affected significantly by the inclusion or exclusion of binaries from the sample.

5. Discussion

Our results show that relatively unevolved stars in h and χ Per (those in group 1 that presumably reflect their initial angular momenta most accurately) rotate on average more rapidly than stars of comparable age in the field by about a factor of 2. The stars with

larger masses in groups 2 and 3 also rotate more rapidly than field stars with similar masses and evolutionary states, but the differences decrease with increasing mass. The differences in mean rotation speed between h and χ Per and the field stars primarily reflect a paucity of slowly rotating stars in the double cluster, particularly among stars in groups 1 and 2. It has been known for a long time (e.g. Slettebak 1968) that there are a large number of Be stars in h and χ Per, and so the fact that we find a bias toward rapidly rotating stars in these clusters is perhaps not surprising. We note as well that the observed distribution of rotation speeds in h and χ Per is unusual compared with other, albeit lower density, clusters (e.g. Brown & Verschueren (1997)).

What causes the differences in N(v *sin* i) between h and χ Per and the field? Is the near absence of slow rotation seen in h and χ Per a consequence of a difference in the initial conditions that characterize the formation of stars in a dense, bound cluster as compared with the presumably lower density regions in which field stars form? If so, what specific differences in initial conditions are the determining factors? Why do the distributions of v *sin* i for h and χ Per stars appear to converge progressively toward the distributions of v *sin* i seen for the field stars in the two hotter regions? Is this apparent convergence the result of processes that are effective after stars reach the ZAMS? Or was the similarity of N(v *sin* i) between h and χ Per and the field found for early B stars imposed at the time of star formation?

5.1. Rotation Changes during Evolution away from the ZAMS

We consider first the question of how evolution affects N(v *sin* i) after stars reach the ZAMS, and specifically whether it is plausible that the massive stars in group 3 initially shared the high average rotation speeds of their cooler, lower mass cohorts in groups 1 and 2, but converged to the field star average as they evolved.

Heger & Langer (2000) and Meynet & Maeder (2000) have calculated models of evolving rotating stars for stars spanning the masses represented among group 3. These models show that qualitatively, as high mass main sequence stars evolve from the ZAMS toward the end of core hydrogen burning, their surface rotation should decrease as a result of (a) changes in stellar moments of inertia; and (b) loss of stellar angular momentum via strong stellar winds. However, the magnitude of the decrease in surface rotation rate is predicted to be modest because the loss of angular momentum from the surface layers is partially compensated by the transport of angular momentum from the core of the star. For a 12 $M\odot$ star, Heger and Langer predict that the rotation rates of stars initially rotating at 300 km s^{-1} or less will decline by only 20-25% during the course of their main sequence lifetimes; surface rotation

begins to increase only after core hydrogen is exhausted and stars approach the terminal age main sequence (TAMS). Stars of this mass whose initial rotation speeds exceed 300 km/sec are predicted to slow by an additional 10% during the first ∼2 Myr after they reach the ZAMS.

Similarly, for a 9 $M\odot$ star rotating initially at 300 km s^{-1}, Meynet and Maeder predict a 27% decrease in $v\ sin\ i$ during main sequence evolution. Since the decrease of rotation speed as the star evolves from the ZAMS to a point just prior to the TAMS is predicted to be nearly identical in percentage terms for stars of differing initial masses and rotation rates (20-30% over the range mass range 9-12 $M\odot$) one might expect some convergence of $<v\ sin\ i>$ for two groups of stars, one of which initially contained a large number of rapid rotators and a second group of stars dominated by slow rotators. However, the convergence predicted from extant models (∼25%) is much smaller than that required to reduce the mean $v\ sin\ i$ by a factor of 2, the amount required to evolve a distribution, N($v\ sin\ i$), similar to that observed for stars in group 1, to one closely resembling that found for group 3.

Observations as well argue against a factor of two decrease in rotation rates as stars evolve. Wolff & Preston (1978) and WEP searched for a correlation between $v\ sin\ i$ and age by sorting field B stars according to the Strömgren β index, which through its sensitivity to surface gravity provides a measure of distance from the ZAMS and hence of age. While this technique is somewhat uncertain since the β index can be affected both by emission and by extremely rapid rotation, these authors found no significant systematic differences in $<v\ sin\ i>$ as a function of distance from the ZAMS, and hence argued that any change in $v\ sin\ i$ with age must be small at least for this heterogeneous sample. Abt (2003) looked for systematic differences in $<v\ sin\ i>$ between B dwarfs and giants of the same masses among a sample of field stars. By using spectral type as a surrogate for mass, Abt reports that for stars of 9 $M\odot$ (the highest mass included in his study) rotation rates decline by only 11% from class V to class III stars. Perhaps the best extant evaluation of age-drive rotation changes is that of Gies & Huang (2003), who observed B0-B3 stars (the spectral type range populating our group 3) in clusters with ages in the range 3-18 Myr. They found evidence for a possible decrease in rotation of about 20% from the ZAMS to ages t ∼10 Myr, followed by an apparent spinup of perhaps 30% among stars older than 10 Myr; this spinup occurs well before the stars reach the TAMS and is not predicted by the models of single rotating stars.

Both theoretical calculations and observations therefore argue against the hypothesis that the early B stars in h and χ Per initially rotated twice as rapidly as their counterparts in the field. Rather, it appears that the differences between h and χ Per and the field stars are intrinsically largest among the late B stars and diminish with increasing mass.

Several authors over the years have reported results similar to those that we find here—namely that stars in clusters rotate more rapidly than stars in the field (e.g. Bernacca & Perinotto 1974; WEP 1982; Gies & Huang 2003; Keller 2004). In the latter two cases, the difference was attributed to evolutionary effects. Gies & Huang suggested that the field stars might represent a population that is somewhat older than their sample of fairly young cluster stars and that spin down processes reduce the average rotation rates of the field stars (as predicted by theory). By contrast, Keller, who reports observations of rotation speeds among LMC clusters with ages greater than 10 Myr, suggests that the higher rotation speeds observed among cluster stars results from LMC clusters having ages systematically larger than their field counterparts. In this case, the spin up among the putatively older LMC cluster sample is attributed to the increase in $<v\ sin\ i>$ expected as stars approach the TAMS.

Both studies selected their samples based primarily on spectral type; as a consequence, the age distributions among the field and cluster samples are not well defined. In the current study, we have been careful to match the ages represented among our field and cluster stars, and in any case we find the largest differences between the field and h and χ Per samples among the late B stars, which are essentially unevolved. Therefore, for the current sample, we cannot attribute the differences in N($v\ sin\ i$) to a systematic difference in age between the cluster stars in h and χ Per and the field stars.

5.2. Initial Conditions and Rotation

The above results suggest that the effects of evolution on observed $v\ sin\ i$ distributions should in principle be small. Hence, the observed differences between h and χ Per and the field seem most logically attributed to differences in initial conditions. Three different types of initial conditions have been cited as factors that influence the observed angular momentum of stars: 1) binary frequency; 2) composition; and 3) environment.

5.2.1. Binary Characteristics

Binary frequency has the potential to influence the rotation of the component stars in two ways. First, closely spaced binaries are expected to have their rotational and orbital motions synchronized. Second, the formation of a binary system, whatever its spacing, may result in a system in which most of the angular momentum resides in orbital motions rather than stellar rotation.

ALG examined the issue of synchronization in their sample of field B stars. They conclude that stars with orbital periods less than 2.4 days rotate synchronously and that stars with periods between 2.4-5 days are synchronized within a factor of two. Moreover, they find that the average rotation observed among stars in close binaries is indeed lower than for apparently single stars, a result expected if orbital and rotational speeds are synchronized (note that for a period of 2.4 days, the corresponding rotational velocity of a typical B star would be 60 km s^{-1}). However, ALG warn that the apparent difference in rotation speeds between binary and single stars might also reflect the fact that stars with published orbits are biased toward sharp-lined stars. For their sample of cluster stars, Gies & Huang also find a difference in the same sense: $<v \sin i>$ = 125 km s^{-1} for stars known to have variable velocities and 168 km s^{-1} for constant stars.

In order to attribute the more rapid rotation seen among the h and χ Per sample to a difference in the effect of synchronization, h and χ Per would have to be deficient in close binaries. The data presented in Table 1 provide an estimate of the number of stars in our h and χ Per sample with instantaneous observed amplitudes K > 30 km s^{-1} based on a comparison of (typically) a single observed radial velocity with the cluster mean. We can use the complete orbital information for the field binaries to estimate what fraction of the field stars would be detected as binaries in a single observation by calculating for each star for which an orbit is known the fraction of time that the observed velocity differs from the average by more than 30 km s^{-1}. Since stars with amplitudes greater than 30 km s^{-1} are all fairly close binaries, we have made the simplifying assumption that their orbits are circular. Column 4 of Table 5 shows the fraction of the field stars either with known orbits and velocity amplitudes K > 30 km/sec or that ALG reported to have double lines. This fraction refers to the number of binary systems; that is, we have counted each binary pair as one system. Column 4 of this table also shows the fraction of binaries with known orbits that would have been detected with a single observation to have a velocity that differed by more than 30 km s^{-1} from the center of mass velocity. This number is to be compared with the fraction in h and χ Per. Given the small number statistics for the h and χ Per sample, there is no evidence for a significant difference in the number of short period binaries between h and χ Per and the field.

As an additional check on our conclusion that a deficiency of close binaries in h and χ Per is not the explanation for their higher mean rotation speeds, we can ask how $<v \sin i>$ for the field stars would change if the field sample contained no close binaries. Reference to Table 5 shows that the fraction of large amplitude (K > 30 km s^{-1}), and therefore close, binaries among the field stars in our three mass intervals ranges from 10-18%. If we calculate $<v \sin i>$ for the total sample including binaries and the sample excluding those stars with velocity variations greater than 30 km s^{-1}, the two averages for each of the three mass intervals

differ by no more than 6% (see Table 4). Based on our analysis of the field star sample, we therefore conclude that even if h and χ Per contained no close binaries, the difference in average rotation speeds between cluster and field samples cannot be explained.

Although the difference in rotation speeds between h and χ Per and field stars cannot be explained by a difference in the fraction of synchronized (close) binaries, recent work by Brown and Verschueren (1997) suggests that the overall frequency of binaries could influence the distribution of *v sin i*. These authors conclude that the binary stars in the loose Sco OB2 association rotate on average more slowly than single stars. However, most of the detected binaries in this survey are so widely separated that one would not expect synchronization to be effective. Brown & Verschueren suggest instead that the observed slow rotation among the Sco OB2 binaries is a result of preferential allocation of angular momentum to orbital motion rather than stellar rotation during the star formation process. It could be that in a dense region like h and χ Per, the formation of widely separated binaries is somehow inhibited by dynamical interactions and as a result there is a deficiency of widely separated binaries relative to what is seen in the field. While such an effect could explain the more rapid rotation seen in h and χ Per, there is at present no way of testing this hypothesis.

5.2.2. Chemical Composition

Studies of rotation among B stars in the Magellanic Clouds have led to the suggestion that stars formed in the lower metalllicity LMC and SMC rotate more rapidly than stars formed in the solar neighborhood. Indirect evidence cited in support of this hypothesis is the observed anti-correlation between the frequency of Be stars, which are rapid rotators, and metallicity (Maeder, Grebel, & Mermilliod 1999). More recently, Keller (2004) has obtained rotational velocities for (a) B0-B2 stars in LMC clusters that have ages between 10 and 30 Myr; and (b) LMC field stars in the same range of spectral types. He concluded that both the LMC field and cluster samples rotate more rapidly than their field star counterparts in the Milky Way; the difference is significant at the 2 σ level.

Differing abundances cannot, however, account for the fact that h and χ Per stars on average rotate more rapidly than Galactic field stars. Vrancken et al. (2000) find that the abundances measured for early B giants in h and χ Per are in reasonable agreement with abundances measured by other authors for main sequence B stars, including nearby field stars.

5.2.3. Possible Relationship between Initial Conditions and ZAMS Rotation Speeds

Field B stars are generally assumed to have formed in loose clusters, associations, or aggregates that disperse rapidly. Since the h and χ Per clusters are still bound, it is reasonable to assume that the stars comprising these clusters were formed in regions of higher average protostellar densities than those characterizing the birthplace of a typical field B star. For reasons noted in the introduction, theory suggests that time-averaged protostellar accretion rates are likely to be higher in denser regions. If the linkage between initial density and protostellar accretion rate predicted by theory is correct, current models predict higher rotation speeds among the outcome stellar populations formed in dense regions.

Suppose that (a) material from a protostellar core infalls onto a disk; (b) material is transported to a forming star through a circumstellar accretion disk; and (c) the inner region of the accretion disk is linked to the star via stellar magnetospheric field lines as described in the introduction. If so, various formulations of the accretion process (e.g. Johns-Krull & Gafford 2002) predict that, for fixed magnetic field strength, the rotation rate should vary directly as a (positive) power of the accretion rate, since higher accretion rates tend to crush the stellar magnetosphere and drive the disk/magnetosphere corotation radius of the disk closer to the surface of the star. The rotation rate at the birthline, i.e. when the phase of rapid accretion ends, also depends directly on a power of the protostellar radius, which in turn also depends on the accretion rate, with larger accretion rates leading to larger radii along the birthline. The combination of higher initial angular velocity and higher initial radius for higher accretion rates, can in principle lead to higher ZAMS rotation speeds following pre-main sequence contraction from the birthline to the ZAMS. This notional linkage—high protostellar accretion rates which lead to high angular rotation speeds along the birthline and, finally, high ZAMS rotation speeds—neglects many important effects: probable complex topology of the magnetic field, the localized structures of the accretion columns, and the differential rotation of the disk and the star, which leads to disconnection of the magnetic field that links the two and reduces the spin-down torque (Matt & Pudritz 2004). Nevertheless, by making plausible assumptions regarding stellar accretion rates in low density star-forming regions, Wolff, Strom, & Hillenbrand (2004) demonstrate that it is possible to account for the observed trends in specific angular momentum with mass for stars in the mass range 0.1-10 $M\odot$.

The large difference in rotation speeds between groups 1 and 2 in h and χ Per and their field analogs may find explanation in the sensitivity of the mass-radius relationship along the stellar birthline to accretion rate over the mass range $M \sim 4 - 12M\odot$., i.e. the mass range observed among the h and χ Per and field B star sample discussed above. Over this range of stellar masses, models of the accretion process predict: (a) that the radius of

the forming star when it is deposited on the birthline is larger for larger accretion rates; but (b) perhaps most significantly, that for all accretion rates, the mass-radius relationship exhibits a sharp maximum in radius at a mass somewhere in the range 4-12 $M\odot$. The local maximum in radius reflects the onset of deuterium shell burning, which produces a substantial expansion in the radius of the accreting protostar; the specific range of masses at which D-shell burning sets in, and the radius expands, depends in turn on the protostellar accretion rate. The potential significance of a local maximum in radius along the birthline for stars having masses somewhere between 4-12 $M\odot$ results from the fact that the rotation rates observed when B stars reach the ZAMS depend on the initial rotation rates at the birthline and the spinup as stars contract from the birthline to the ZAMS.

We speculate that the large difference between h and χ Per stars and the field among groups 1 and 2 reflects a difference in the mass accretion rates characterizing the cluster (high accretion rate) and field birthplaces (low accretion rate) that in turn produces differences in initial radii along the birthline that are largest among stars having masses in the range 4.5 to 9 $M\odot$. If correct, stars in this mass range should show the largest difference in rotation speeds—a direct result of greater spinup during contraction toward the ZAMS. At higher masses, the difference in rotation speeds between cluster and field should be smaller, since the initial radii along the birthline are similar or, for those stars where the birthline meets the ZAMS, identical.

6. Conclusions

Observations of rotational velocities show that B stars in the h and χ Per double cluster rotate on average more rapidly than field stars of the same mass and age. This result combined with other similar results in the literature clearly establishes that the rotation rates of B stars *differ significantly* among stars born in different regions. We have argued that the observed differences are *likely* built in at the time the stars were formed and not a consequence of subsequent evolutionary processes. Since h and χ Per are currently bound clusters, it seems reasonable to assume that stars in these clusters were formed in much denser environments than field B stars of comparable age, which have presumably escaped from the loose clusters, associations, or small groups in which they formed. We have identified two possible explanations for the observed differences in rotation speeds, each related to the density at the time of star formation. One hypothesis is essentially untestable with current facilities: that h and χ Per are deficient in wide binaries relative to the field and that when wide binaries are formed, much of the available angular momentum appears as orbital rather than stellar rotational angular momentum. The second possibility is that protostellar

accretion is more rapid in higher density regions, and that high accretion rates lead to more rapid rotation—a consequence of the hypothesis that "disk locking"" accounts for initial stellar angular momenta. This hypothesis is attractive because the effects of differences in accretion rate during the stellar assembly phase are predicted to be particularly dramatic among B stars. For stars in the mass range 4-12 $M\odot$, the initial radius along the stellar birthline reflects the effects of deuterium shell burning, which causes a substantial expansion of the star; the amount of the expansion and the range of stellar masses over which it occurs both increase with increasing accretion rates. The combination of high initial accretion rate with high initial radius followed by contraction from the birthline to the ZAMS can lead to high ZAMS rotation speeds compared to stars of similar mass formed in regions characterized by lower accretion rates.

We emphasize that our results for h and χ Per, while suggestive, do not provide conclusive evidence of a direct relationship between environment and outcome rotational velocities. With the advent of 8- to 10-m telescopes, it should be possible to test the hypothesis that outcome stellar rotation speeds are in fact linked to initial stellar density among stars born in a wide variety of environments by observing a large sample of stars located in young clusters both the in Milky Way and in the Magellanic Clouds. Such observations will provide the basis for establishing robustly both the cosmic dispersion in N(vsini) as well as systematic differences attributable to initial stellar density, chemical composition, or other parameters. For regions of sufficient youth, it may also be possible to search for differences in the location of the birthline. If the predicted correlations between rotation speed, birthline location, and environment can be found, it would be possible for the first time to link the initial conditions under which star formation takes place and to outcome observables—a crucial first step toward a predictive theory of star formation.

Facilities: WIYN.

REFERENCES

Abt, H.A. 2003, ApJ, 582, 420
Abt, H.A., & Hunter, J.H., Jr. 1962, ApJ 136, 381
Abt., H.A., Levato, H., & Grosso, M. 2002, ApJ 573, 359 (ALG)
Bernacca, P.L., & Perinotto, M. 1974, A&A, 33, 443
Bragg, A.E., & Kenyon, S.J. 2002, AJ, 124, 3289
Brown, A.G.A., & Verschueren, W. 1997, A&A, 319, 811
Capilla, G., & Fabregat, J. 2002, A&A, 394, 479
Collins, G.W. & Sonneborn, G.H. 1977, ApJS, 34.41

Crawford, D.L. 1978, AJ, 83, 48
Crawford, D.L., Glaspey, J.W., & Perry, C.L. 1970, A. J., 75, 822
Drilling, J.S., & Landolt, A.U. 2000, in Allen's Astrophysical Quantities, ed. A. N. Cox (4th ed.; New York: AIP), 381
Elmegreen, B. G.; Shadmehri, M. 2003, MNRAS 338, 817
Gies, D.R., & Huang, W. 2003, IAU Symposium No. 215, in press
Heger, A., & Langer, N. 2000, ApJ, 544, 1016
Hauck, B. & Mermilliod, M. 1998, A&A Suppl. Ser, 129, 431
Johns-Krull, C. M., & Gafford, A. D. 2002, ApJ, 573, 685
Keller, S. C. 2004, PASA, in press (astro-ph/0405129)
Keller, S.C., Grebel, E.K., Miller, G.J., & Yoss, K.M. 2001, AJ, 122, 248
Königl, A. 1991, ApJ Letters 370, 39
Maeder, A., Grebel, E.K., & Mermilliod, J.-C. 1999, A&A, 346, 459
Massey, P., & Hunter, D.A. 1998, ApJ. 493, 180
Matt, S., & Pudritz, R. E. 2004, ApJ, 607, L43
McKee, C. F., & Tan, J. C. 2003, ApJ 585, 850
Meynet, G., & Maeder, A. 2000, A&A, 361, 101
Schaller, G., Schaerer, D., Meynet, G., & Maeder, A. 1992, A&AS, 96, 269
Shu, F. H., Najita, J., Ruden, S. P., & Lizano, S. 1994, ApJ, 429, 797
Sirianni, M., Nota, A., Leitherer, C., DeMarchi, G., & Clampin, M. 2000, ApJ, 533, 203
Slesnick, C.L., Hillenbrand, L.A., & Massey, P. 2002, ApJ 576, 880 (SHM)
Slettebak, A. 1968, ApJ 154, 933
Slettebak, A. 1985, ApJS, 59, 780
Slettebak, A., Collins, G.W.II, Parkinson, T.D., Boyce, P.B., & White, N.M. 1975, ApJS, 29, 137
Stahler, S.W. 1988 ApJ 332, 804
Stolte, A., Grebel, E.K., Brandner, W., & Figer, D.F. 2002, A&A 394, 459
Townsend, R.H.D., Owocki, S. P., & Howarth, I. D. 2004, MNRAS, 350, 189
Vrancken, M., Lennon, D. J., Dufton, P. L., & Lambert, D. L. 2000, A&A, 358, 639
Wolff, S.C., & Preston, G.W. 1978, ApJSuppl., 36, 497
Wolff, S. C., Edwards, S., & Preston, G. W. 1982, ApJ 252, 322 (WEP)
Wolff, S.C., Strom, S. E., & Hillenbrand, L.A. 2004, ApJ, 601, 979

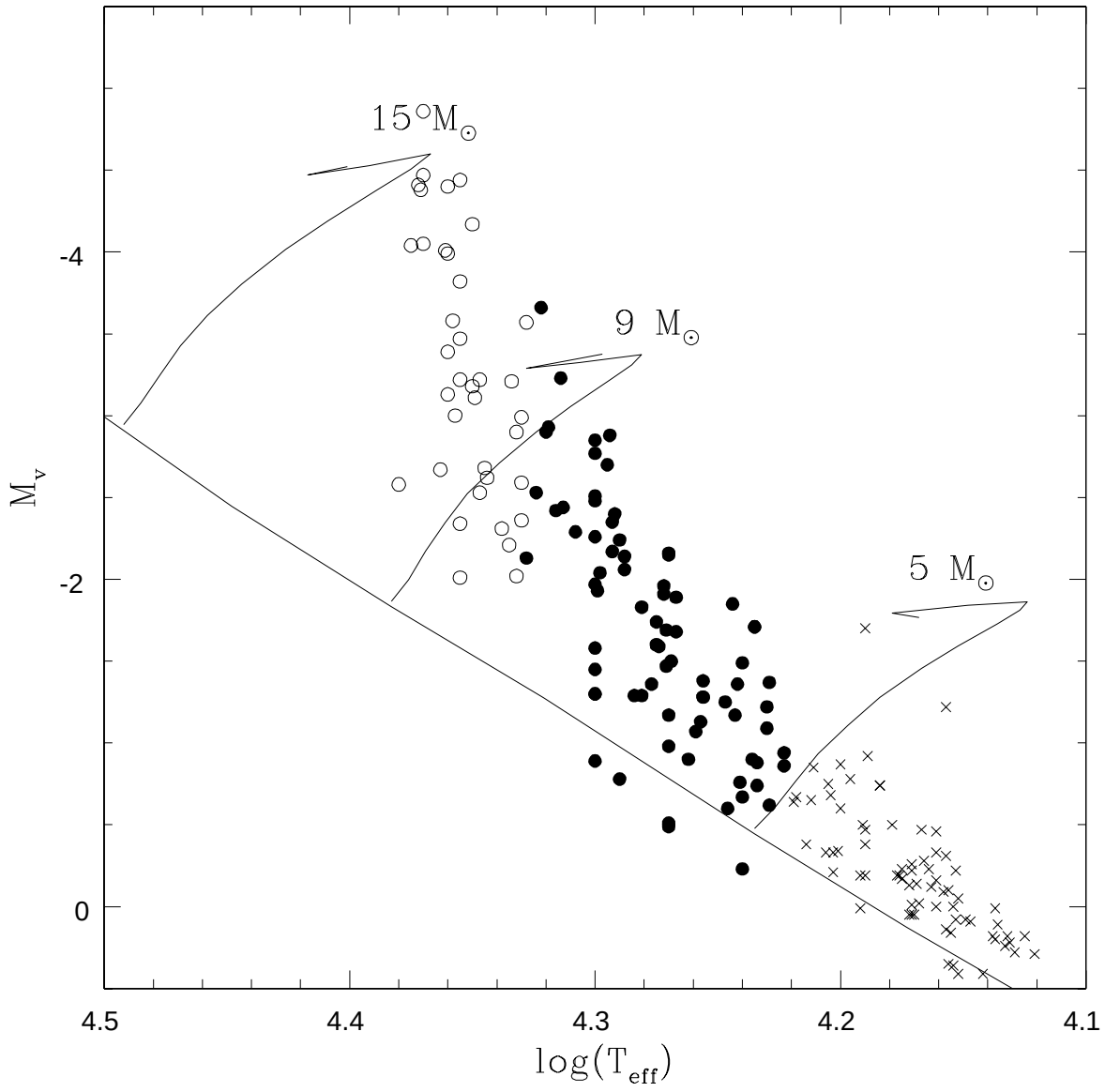

Fig. 1.— The M_v vs. log T_{eff} diagram for the stars in h and χ Per. The data are from Slesnick, Hillenbrand, & Massey (2001). For analysis, these stars have been divided according to T_{eff} into three groups, represented from hottest to coolest by the open circles, filled

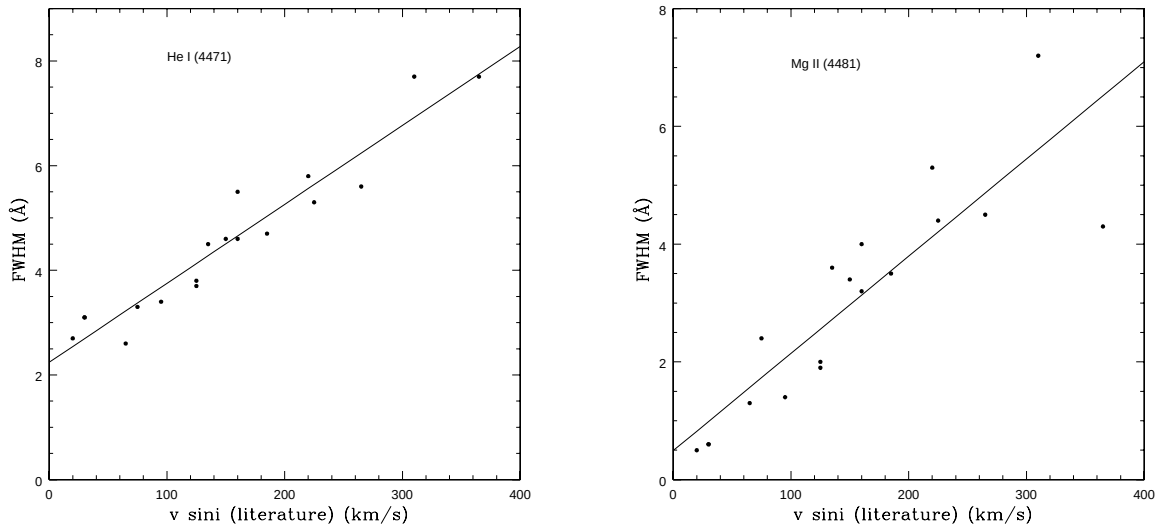

Fig. 2.— The relationships between FWHM of He I λ 4471 (left) and Mg II λ 4481 (right) and *v sin i* for standard stars in I Lac (Abt & Hunter 1962). The best least squares fit to the data is shown in each panel.

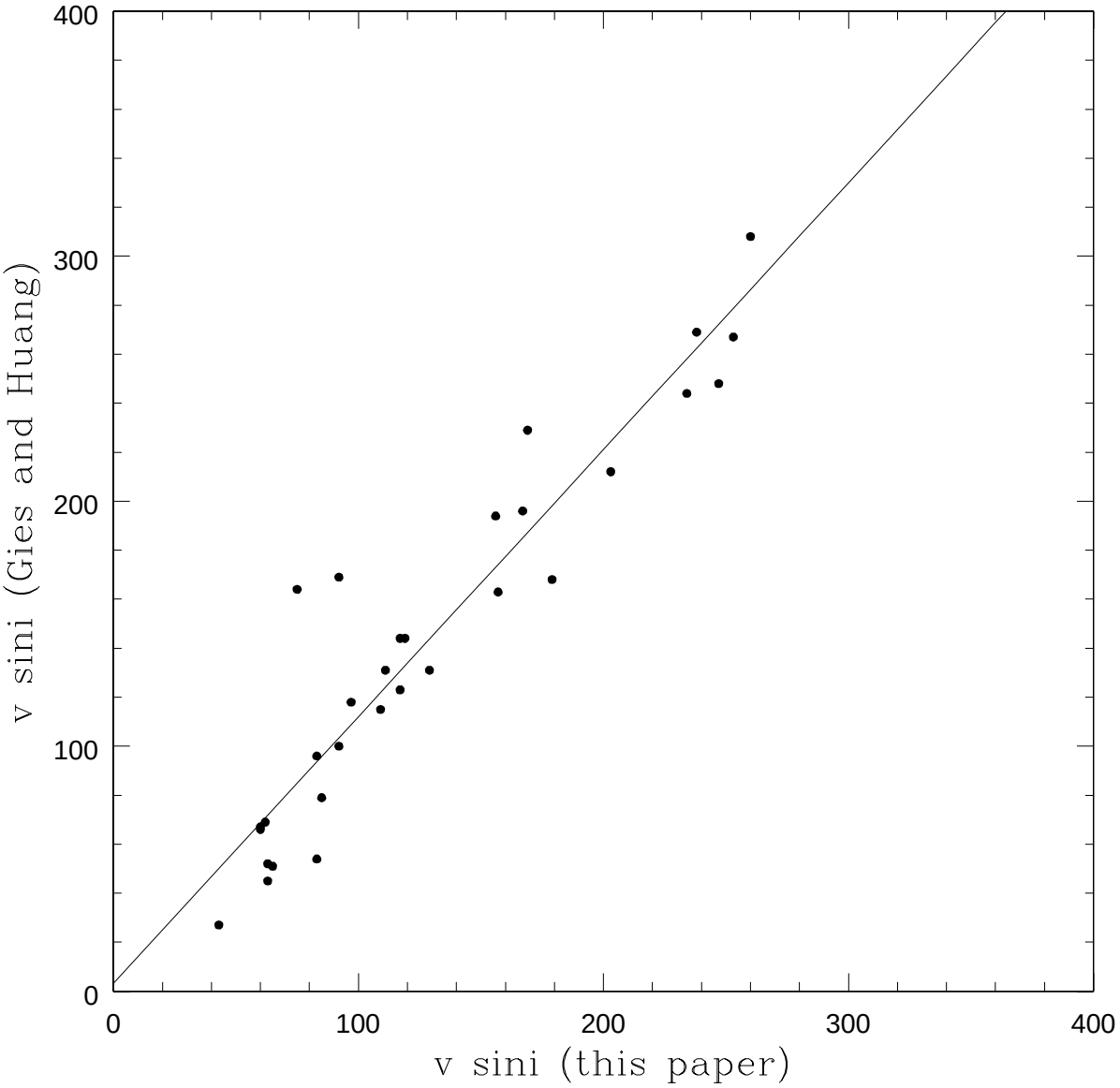

Fig. 3.— The comparison between the values of *v sin i* measured in the current study and those derived by Gies & Huang (in preparation) for stars in h and χ Per that are common to the two programs. The best fitting straight line is given by $vsini(Gies\&Huang) =$

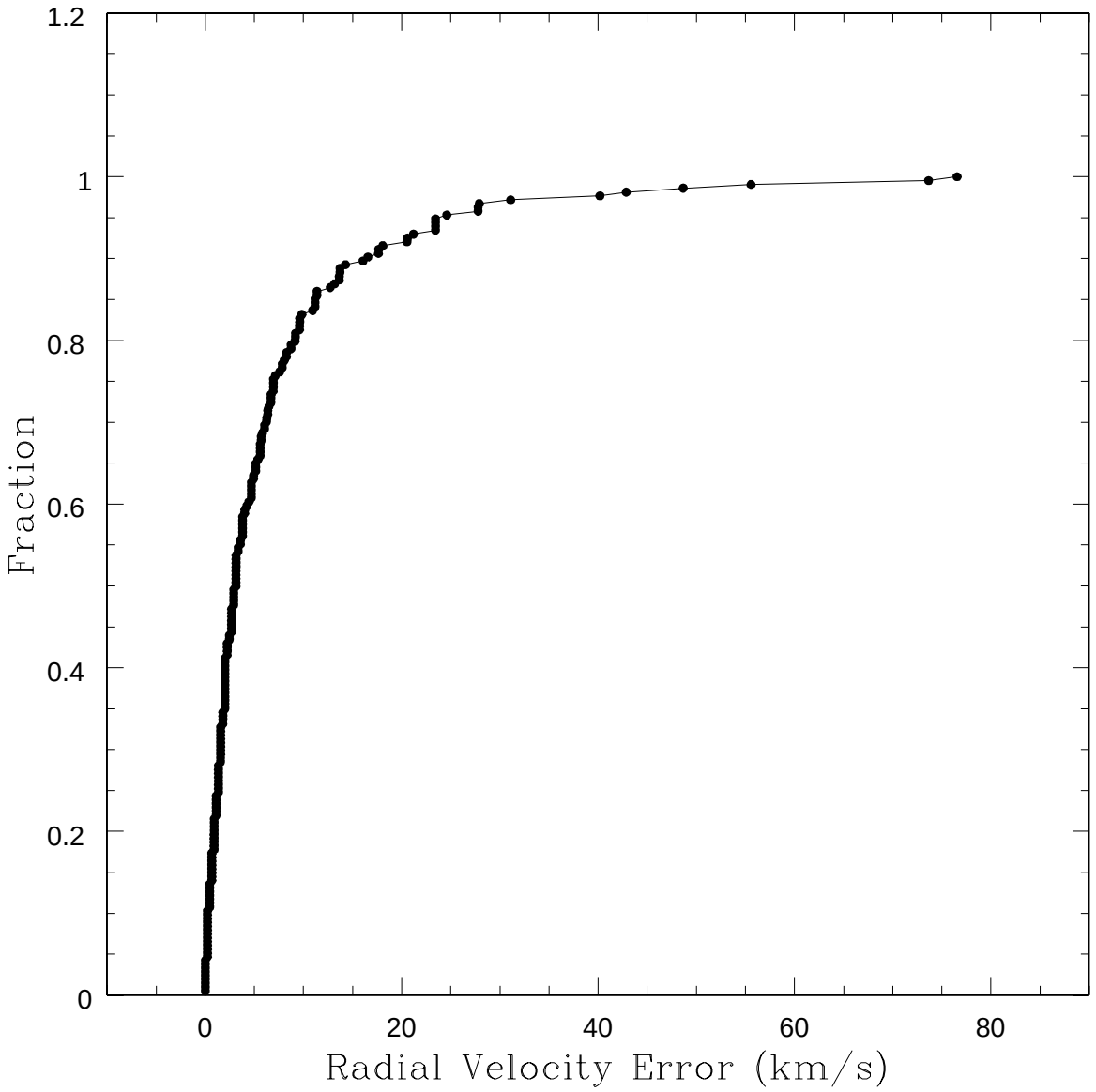

Fig. 4.— The cumulative distribution of velocity differences between pairs of exposures of the same stars taken less than 45 minutes apare. Since radial velocity should not change significantly over this short interval of time, the differences can be taken as an estimate of the

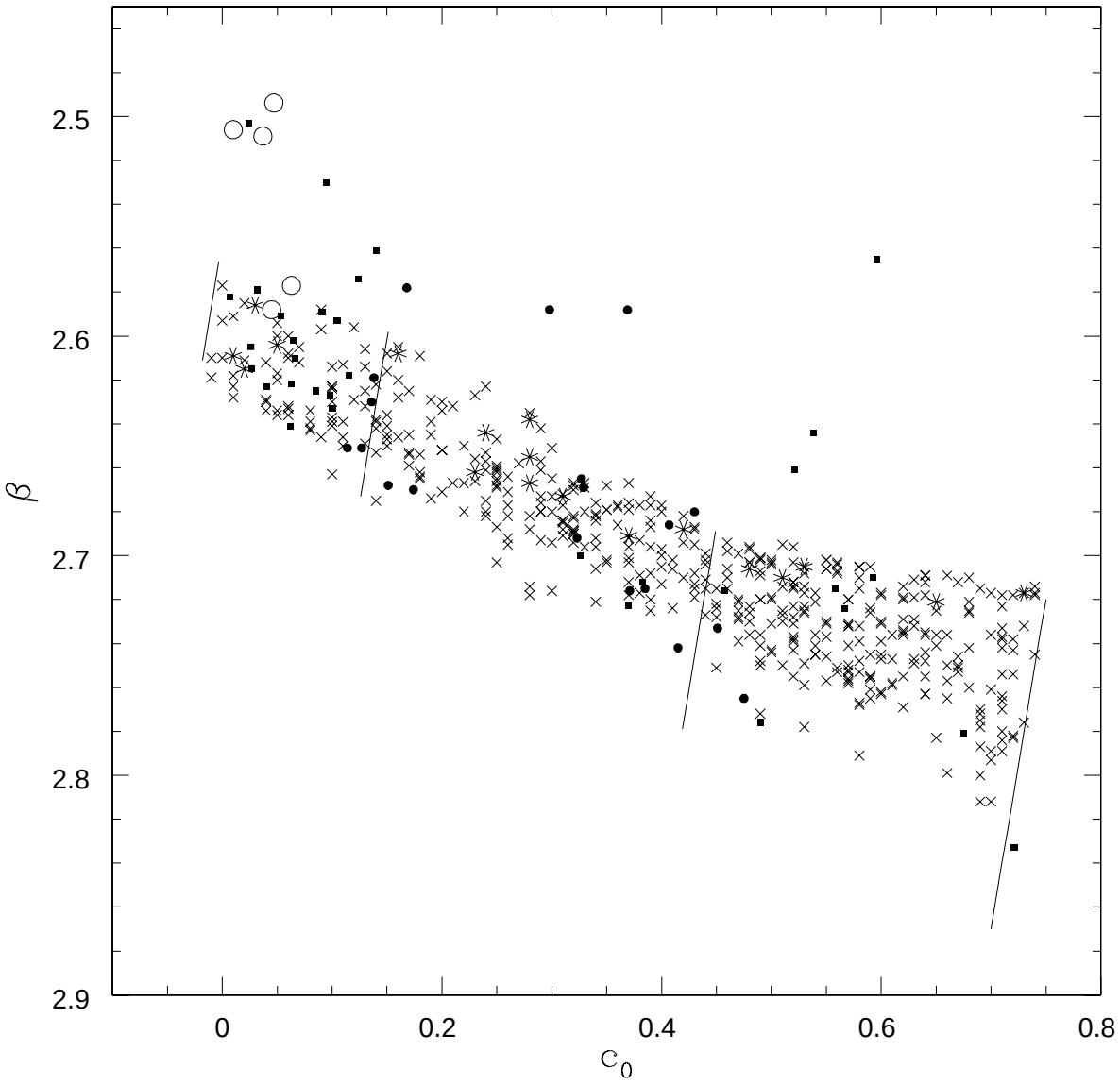

Fig. 5.— Measured values of β and c_0 for ALG field stars included in our sample (crosses). The boundaries between groups are shown as solid lines. Dots represent measurements for that subset of the h and χ Per sample with published photometry; open circles indicate

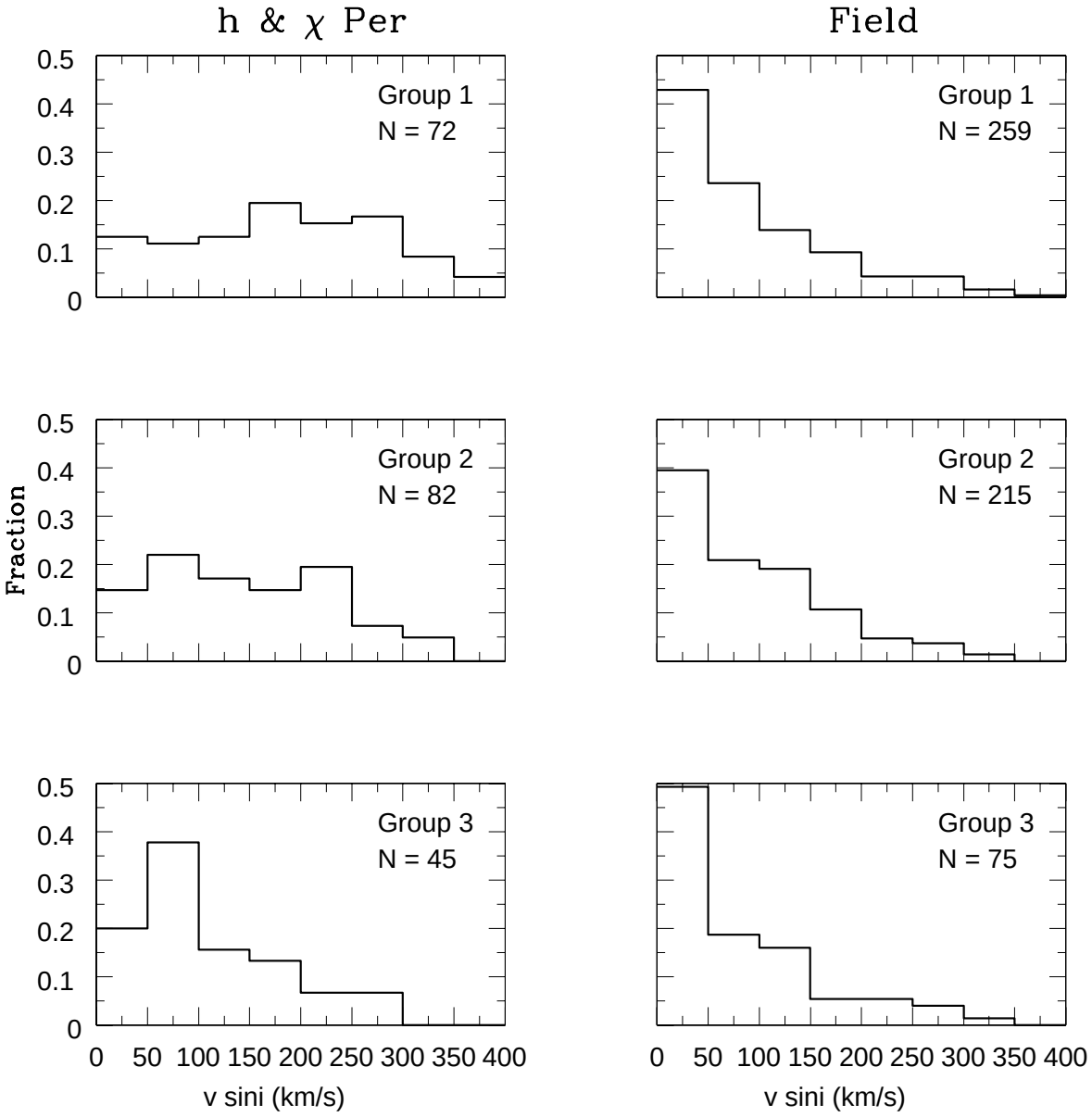

Fig. 6.— Distribution of $v \; sin \; i$ for each of the three groups of stars in h and χ Per compared with the distributions for field stars. Note the large differences in the distributions for the stars in the coolest group (Group 1) and the progressive convergence of the distributions

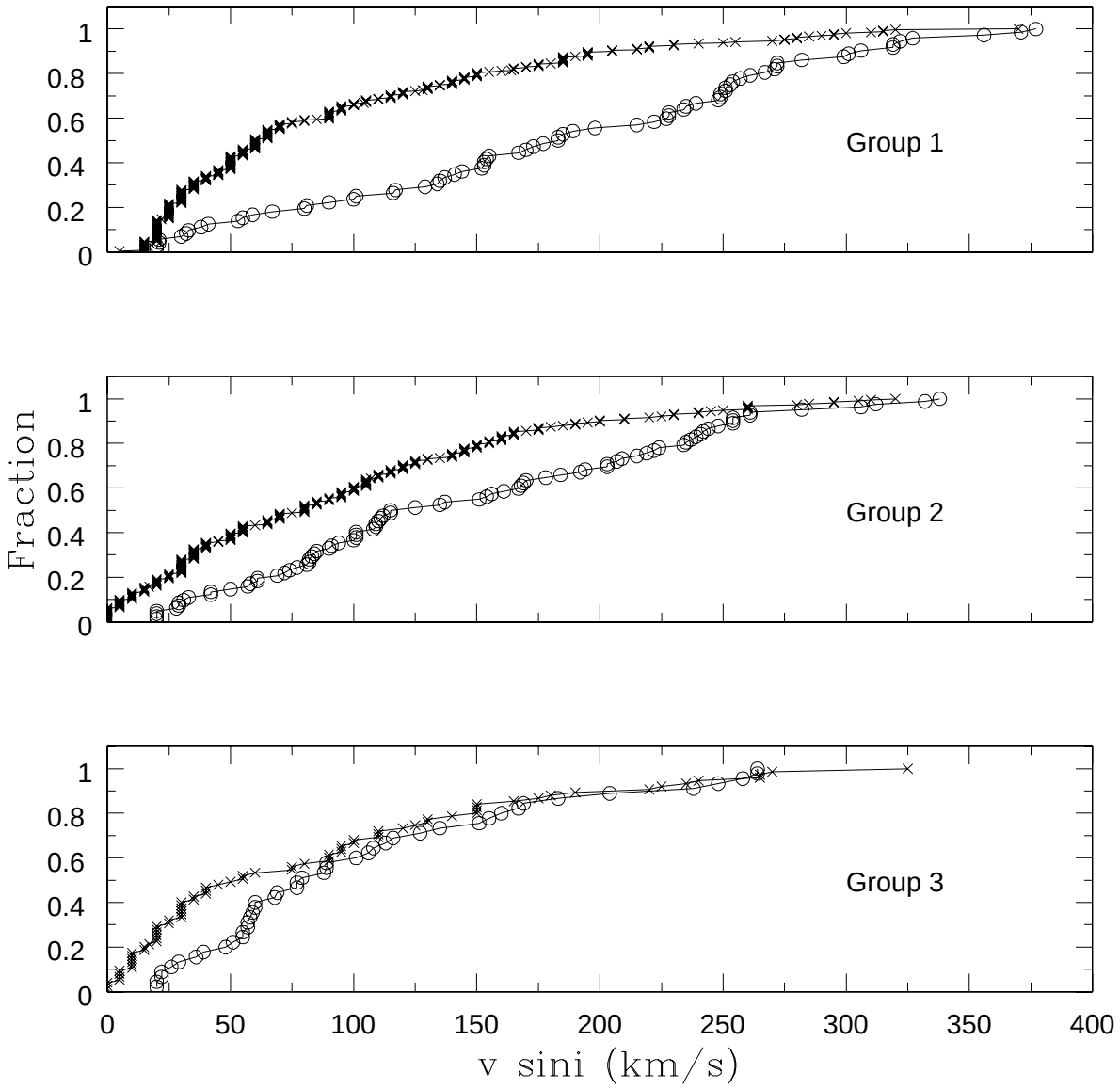

Fig. 7.— Cumulative distribution of $v\ sin\ i$ for the stars in h and χ Per (open circles) compared with the distributions for field stars (crosses) of similar temperature and age. Stars of Group 1 comprise late B stars, little evolved from the ZAMS. Stars of Group 2

Table 1. Data for Stars in h and χ Persei

ID	Oosterhoff	M_v	Log(T_{eff})	Sp. Type	Mass (Sun=1)	*v sin i* (km s^{-1})	Group	c_0	β	Binarity
9	2227	-5.57	4.375	B1.5II	21	22	—	0.031	2.584	
12	662	-4.86	4.37	B1.5I	16.4	22	3	0.007	2.582	
16	1132	-5.12	4.34	B2I	16.8	60	—			
19	2296	-4.79	4.34	B2I	15.1	146	—	0.05	2.598	
28	847	-4.47	4.37	B1.5Ie	15.2	55	3	0.063	2.577	
32	2299	-4.05	4.37	B1.5I	13.2	106	3	0.027	2.615	
33	2371	-4.44	4.355	B2III	14	60	3	0.024	2.503	delta v = -62
36	2541	-4.4	4.36	B1.5III	14.4	55	3	0.066	2.61	
40	1116	-4.65	4.45	B0.5V	20	93	—	0.088	2.635	
41	2088	-4.41	4.372	B1IIIe	14.8	89	3	0.01	2.506	
42	717	-4.09	4.405	B1V	15	57	3	0.026	2.605	delta v = 40
43	843	-4.17	4.35	B1.5V	13.2	88	3	0.091	2.589	
46	1268	-4.38	4.371	B0.5V	14.6	127	3	0.032	2.579	
47	2311	-4.04	4.375	B1.5II	13.3	20	3	0.065	2.602	
49	692	-3.81	4.44	B0.5I	15.5	169	3			
52	782	-3.99	4.36	B1.5III	12.7	36	3	0.095	2.53	
54		-4.01	4.361		12.9	116	3			
57	922	-4.15	4.397	B2V	14.2	258	3	0.053	2.591	
58	1261	-4.72	4.502	B3Ve	24	261	—			
66	2284	-4.24	4.484	Be	19.7	299	—	-0.082	2.381	
71	980	-3.82	4.355	B2III	12	39	3	0.098	2.627	
72	1078	-3.81	4.405	B1V	14.1	167	3	0.1	2.633	
77		-3.56	4.418		13.8	108	3			
78	1364	-3.66	4.322		11.1	203	2			
81	864	-3.57	4.328	B2V	10.8	113	3	0.14	2.561	
83	2246	-3.47	4.355	B2III	11.5	101	3	0.04	2.623	
87	517	-3.25	4.267	Be	8.8	178				
91		-3.58	4.358		11.3	264	3			
96	2165	-3.5	4.405	B1Ve	13.2	79	3	0.047	2.494	
100	1161	-3.73	4.405	B1Ve	13.8	135	3	0.045	2.588	
102		-3.11	4.349		10.6	58	3			
106	929	-3.39	4.36	B1.5III	11.5	151	3	0.115	2.618	
109		-3.23	4.314		9.6	161	2			
117	936	-3.18	4.35	B1.5V	10.8	26	3	0.063	2.622	

Table 1—Continued

ID	Oosterhoff	M_v	$Log(T_{eff})$	Sp. Type	Mass (Sun=1)	*v sin i* (km s^{-1})	Group	c_0	β	Binarity
120	1085	-3.22	4.355	B2III	10.9	59	3	0.062	2.641	
121		-3.22	4.347		10.8	20	3			
131	2262	-3.13	4.36	B1.5III	10.9	204	3	0.124	2.574	
133		-3.05	4.389		11.6	248	3			
138		-2.9	4.32		9.5	115	2			
141	2566	-3.21	4.334	Be	10.4	183	3			delta v = -44
144	978	-2.99	4.33	B2IV	9.8	29	3	0.085	2.625	
149		-2.9	4.332		9.8	77	3			
150		-2.67	4.363		10.1	22	3			
158	859	-2.85	4.3	B2V	9	192	2	0.168	2.578	
160		-2.88	4.294		9	156	2			
163		-2.93	4.319		9.5	20	2			
165		-2.68	4.345		9.7	60	3			
171	622	-2.34	4.355	B2III	9.4	57	3			
177		-2.53	4.347		9.5	77	3			
178	2185	-2.59	4.33	B2IV	9.2	155	3	0.326	2.7	
184		-3	4.357		10.6	48	3			
188		-2.42	4.316		8.6	33	2			
189	1282	-2.58	4.38	Be	10.4	264	3	0.037	2.509	
191	1109	-2.77	4.3	B2V	8.9	170	2	0.174	2.67	
193	919	-2.97	4.294		8.5	94	2			
194		-2.08	4.218	B5II	6.7	67	—			
198		-2.7	4.295		8.7	57	2			
200	963	-2.26	4.3	B2.5II	8.1	29	2	0.114	2.651	
201		-2.53	4.324		9	72	2			
202	2114	-2.48	4.3	B2V	8.4	169	2			
203	2232	-2.15	4.27	B3V	7.5	101	2	0.127	2.651	
205		-2.35	4.293		8.1	215	2			
206		-2.17	4.293		7.9	209	2			
208	1041	-2.51	4.3	B2V	8.5	154	2	0.151	2.668	
219	892	-2.24	4.29	B2.5III	7.9	61	2	0.136	2.63	
222		-2.44	4.313		8.6	31	2			
223		-2.21	4.335		8.8	238	3			
231		-2.62	4.344		9.5	51	3			

Table 1—Continued

ID	Oosterhoff	M_v	Log(T_{eff})	Sp. Type	Mass (Sun=1)	*v sin i* (km s^{-1})	Group	c_0	β	Binarity
235	950	-2.36	4.33	B2IV	8.8	89	3	0.105	2.593	
237		-2.4	4.292		8.2	312	2			
239	2229	-2.16	4.27	B3V	7.5	235	2			
240		-2.29	4.308		8.3	242	2			
241		-2.13	4.328		8.5	137	2			
265		-1.83	4.281		7.3	261	2			
277		-2.14	4.288		7.8	109	2			
280		-2.02	4.332		8.5	69	3			
284		-2.01	4.355	B2III	9	68	3			
288	879	-1.97	4.3	B2V	7.8	91	2	0.138	2.619	
289		-1.96	4.272		7.3	194	2			
297		-2.31	4.338		9	160	3			
298		-1.93	4.299		7.7	112	2			delta v = -41
299		-2.04	4.298		7.8	254	2			
314	2091	-2.06	4.288	Be	7.7	167	2			
315		-1.89	4.267		7.1	239	2			
318		-1.85	4.244		6.8	110	2			
331		-1.71	4.235		6.5	42	2			SB2; delta v=106
331		-1.71	4.235		6.5	20	2			SB2
338		-1.69	4.271		7	50	2			
341		-1.74	4.275		7.1	178	2			
350		-1.68	4.267		6.9	82	2			
359	2140	-1.7	4.19	B5V	6	72	—			
362		-1.91	4.272		7.2	101	2			
363		-1.47	4.271		6.8	338	2			
369	2301	-1.58	4.3	B2V	7.4	135	2			delta v = 31
393	778	-1.55	4.35	B1.5V	8.4	225		0.293	2.571	
394	869	-1.45	4.3	B2V	7.3	254	2	0.407	2.686	
401	952	-1.36	4.242		6.3	219	2	0.323	2.692	
404		-1.59	4.274		7	42	2			
409		-1.5	4.269		6.8	237	2			
415		-1.49	4.24		6.4	125	2			
431		-1.29	4.284		6.8	207	2			
436	2379	-1.3	4.3	B2V	7.1	244	2			

Table 1—Continued

ID	Oosterhoff	M_v	Log(T_{eff})	Sp. Type	Mass (Sun=1)	*v sin i* (km s^{-1})	Group	c_0	β	Binarity
439	800	-1.3	4.3	B2V	7.2	234	2	0.298	2.588	
443		-1.6	4.275		7	28	2			SB2; delta v=111
443		-1.6	4.275		7	20	2			SB2
444		-0.78	4.196		5.3	267	1			
450		-1.25	4.247		6.3	77	2			
452	2352	-1.22	4.23	B3III	6	74	2			
453		-1.36	4.277		6.8	109	2			
460		-1.29	4.281		6.8	69	2			
494		-0.96	4.129		4.9	169	—			
497		-1.09	4.23		5.9	101	2			
500		-1.07	4.259		6.3	241	2			
501		-1.38	4.256		6.5	100	2			
506		-0.9	4.236		5.9	90	2			delta v = -67
507		-1.28	4.256		6.4	29	2			SB2; delta v=104
507		-1.28	4.256		6.4	20	2			SB2
513	896	-1.17	4.35	B1.5V	7.9	403	—	0.344	2.649	
514		-1.22	4.157		5.2	21	—			
517		-1.37	4.229		6.1	111	2			
520	956	-1.17	4.243		6.2	83	2	0.371	2.716	
531		-0.74	4.234		5.7	168	2			
533		-0.98	4.323		7.2	196	—			
537		-0.92	4.189		5.3	137	1			
540	965	-1.17	4.27	B3V	6.5	82	2	0.329	2.669	
543		-0.74	4.184		5.1	20	1			SB2; delta v=126
543		-0.74	4.184		5.1	20	1			SB2
549		-1.13	4.257		6.3	248	2			
551		-0.87	4.2		5.4	271	1			
554		-0.75	4.205		5.4	141	1			
562		-0.86	4.286		6.5	81	2			
565		-0.88	4.234		5.8	61	2			
576	876	-0.98	4.27	B3V	6.4	115	2	0.327	2.665	
587		-0.94	4.223		5.7	306	2			
590		-0.5	4.179		4.9	53	1			
594		-0.62	4.229		5.6	85	2			

Table 1—Continued

ID	Oosterhoff	M_v	Log(T_{eff})	Sp. Type	Mass (Sun=1)	*v sin i* (km s^{-1})	Group	c_0	β	Binarity
598		-0.46	4.161		4.7	215	1			
600		-0.65	4.212		5.4	32	1			
602	2349	-0.78	4.29	B2.5V	6.5	261	2	0.43	2.68	
611		-0.5	4.116		4.4	237	—			
616		-0.9	4.262		6.2	254	2			
628		-0.86	4.223		5.7	58	2			
632		-0.85	4.211		5.5	248	1			
641		-0.64	4.219		5.5	299	1			
650	872	-0.89	4.3	B2V	6.8	332	2	0.369	2.588	
655	2297	-0.47	4.19	B5V	5	254	1	0.383	2.712	
658	2211	-0.49	4.27	B3V	6	282	2	0.475	2.765	
670		-0.22	4.153		4.5	30	1			
675	659	-0.38	4.19	B5V	5	153	1			
681		-0.47	4.167		4.8	239	1			
683	2345	-0.51	4.27	B3V	6	108	2	0.415	2.742	
687		-0.76	4.241		5.8	203	2			
701		-0.33	4.206		5.1	67	1			
709	923	-0.21	4.203		5	38	1	0.37	2.723	
721	2275	-0.6	4.246		5.8	184	2	0.385	2.715	
726		-0.33	4.161		4.7	33	1			
736	1066	-0.6	4.2		5.2	153	1	0.458	2.716	
749		-0.38	4.214		5.2	251	1			
753		-0.21	4.123		4.3	207	—			
754	820	-0.23	4.164	BV	4.6	319	1	0.521	2.661	
765		-0.68	4.204		5.3	185	1			
767		-0.31	4.157		4.6	177	1			
768		-0.67	4.218		5.5	144	1			
774		-0.67	4.24		5.7	151	2			
778		-0.58	4.274		6.1	84	2			
782	2267	-0.19	4.19	B5V	4.8	154	1	0.49	2.776	
783		0.01	4.137		4.3	117	1			
792	2350	-0.23	4.24		5.4	222	2	0.451	2.733	
814		-0.07	4.114		4.1	219	—			
853		-0.34	4.201		5.1	101	1			

Table 1—Continued

ID	Oosterhoff	M_v	Log(T_{eff})	Sp. Type	Mass (Sun=1)	$v \sin i$ (km s^{-1})	Group	c_0	β	Binarity
854		-0.26	4.171		4.7	155	1			
859		-0.5	4.191		5	198	1			
862		-0.17	4.175		4.7	90	1			
870		-0.09	4.158		4.5	377	1			
878		-0.22	4.171		4.7	282	1			delta v = -43
884		-0.13	4.172		4.6	235	1			
892		-0.16	4.161		4.6	183	1			
893		-0.28	4.166		4.7	253	1			delta v = -38
896	804	-0.1	4.156		4.5	301	1	0.538	2.644	
903		-0.19	4.192		4.9	59	1			
918	2111	-0.14	4.169		4.6	173	1	0.567	2.724	
920		-0.19	4.177		4.7	81	1			
939		0	4.154		4.4	306	1			
940		0	4.161		4.5	167	1			
941		0.14	4.157		4.4	134	1			
942		-0.33	4.203		5.1	222	1			
952	2116	-0.12	4.163	B8V	4.6	116	1	0.593	2.71	
954	830	-0.25	4.27	B3V	5.8	224	2			
970	784	-0.02	4.168	B8V	4.6	228	1	0.596	2.565	
973		-0.19	4.176		4.7	170	1			
986		0.09	4.147		4.3	322	1			
1007		-0.23	4.175		4.7	319	1			delta v = -41:
1009		0.05	4.171		4.5	327	1			
1017		0.18	4.125		4.1	189	1			
1018		-0.05	4.152		4.4	80	1			delta v = -37:
1040		0.08	4.153		4.4	272	1			
1053		-0.01	4.171		4.6	356	1			delta v = 76
1102		0.18	4.132		4.2	257	1			
1124		0.22	4.131		4.1	249	1			
1128	2426	0.28	4.129	B8V	4.1	261	1			delta v = 32
1140		0.08	4.149		4.3	249	1			
1141		-0.11	4.223		5.1	272	1			
1169		0.35	4.156		4.2	55	1			
1170		0.2	4.137		4.2	251	1			

Table 1—Continued

ID	Oosterhoff	M_v	Log(T_{eff})	Sp. Type	Mass (Sun=1)	$v\ sin\ i$ (km s^{-1})	Group	c_0	β	Binarity
1172	1077	0.11	4.136		4.2	129	1	0.675	2.781	
1176		0.01	4.192		4.8	41	1			
1216		0.24	4.133		4.1	228	1			delta v = -44:
1218		0.05	4.17		4.5	371	1			
1234	1049	0.05	4.172		4.5	152	1	0.558	2.715	
1250		0.18	4.138		4.2	234	1			
1271		0.29	4.121		4	100	1			
1280		0.16	4.155		4.3	21	1			
1294		0.36	4.154		4.2	135	1			
1403		0.41	4.142		4.1	227	1			
1405	1118	0.32	4.128		4	183	1	0.721	2.833	
1518		0.41	4.152		4.2	21	1			delta v = 50

Table 2. Data for Field Stars

HR	HD	Sp. Type	*v sin i* (km s^{-1})	β	c_0
Group 1					
15	358	B8IVmnp	50	2.743	0.52
28	584	B7IV	15	2.757	0.55
61	1256	B6III/IV	150	2.741	0.49
70	1438	B8V	20	2.751	0.67
78	1606	B7V	104	2.737	0.52
96	2054	B9IV	40	2.775	0.69
121	2729	B6V	95	2.709	0.49
123	2772	B8Vn	220	2.754	0.71
137	3038	B9III	195	2.778	0.69
144	3240	B7III	60	2.75	0.67
149	3322	B8IIImnp	25	2.732	0.58
223	4636	B9III	95	2.739	0.58
326	6676	B8V	120	2.742	0.71
345	6972	B9IV	100	2.812	0.70
348	7019	B7III-IV	60	2.741	0.65
364	7374	B8III	25	2.747	0.60
369	7546	B9IIIsp	25	2.719	0.62
438	9298	B7IIImnp	50	2.739	0.60
491	10425	B8IIIn	240	2.715	0.69
561	11857	B5III	25	2.717	0.54
562	11905	B8III	40	2.71	0.58
612	12767	B9.5sp	45	2.714	0.51
677	14272	B8V	25	2.763	0.64
682	14392	B9sp	90	2.772	0.49
702	14951	B7IV	215	2.727	0.51
746	16004	B9mnp	30	2.753	0.56
760	16219	B5V	30	2.72	0.49
785	16727	B7IIIp	20	2.729	0.47
811	17081	B7IV	25	2.717	0.60
836	17543	B6V	70	2.703	0.48
846	17743	B8III	50	2.741	0.57
847	17769	B7V	145	2.741	0.54
873	18296	B9p	25	2.767	0.58
890	18537	B7V	90	2.739	0.52
896	18604	B6III	105	2.72	0.57
910	18883	B7V	65	2.758	0.57
954	19832	B6IV-V	110	2.746	0.55
982	20315	B8V	185	2.736	0.65
1038	21364	B9Vn	195	2.783	0.65
1047	21455	B7V	120	2.731	0.55
1051	21551	B8V	295	2.746	0.67
1094	22316	B9p	150	2.778	0.53
1097	22402	B8Vn	320	2.731	0.60
1100	22470	B8/B9III	128	2.728	0.47

Table 2—Continued

HR	HD	Sp. Type	*v sin i* (km s^{-1})	β	c_0
1113	22780	B7Vne	230	2.705	0.53
1140	23288	B7IV	185	2.749	0.63
1141	23300	B6V	20	2.702	0.49
1144	23324	B8V	185	2.748	0.64
1145	23338	B6IV	105	2.702	0.55
1146	23363	B7V	140	2.735	0.64
1172	23753	B8V	290	2.737	0.71
1202	24388	B8V	135	2.736	0.61
1207	24504	B6V	130	2.721	0.47
1213	24587	B5V	30	2.744	0.50
1243	25330	B5V	140	2.724	0.45
1305	26670	B5Vn	270	2.715	0.46
1307	26676	B8Vn	175	2.748	0.58
1315	26793	B9Vn	275	2.732	0.73
1328	27026	B9V	220	2.783	0.72
1363	27563	B5III	35	2.703	0.52
1375	27742	B8IV-V	175	2.763	0.64
1377	27777	B8V	250	2.744	0.64
1397	28114	B6IV	25	2.698	0.46
1399	28149	B7V	115	2.726	0.48
1402	28217	B8IV	60	2.717	0.53
1424	28503	B8V	60	2.73	0.55
1445	28929	B9p	55	2.749	0.53
1449	29009	B9sp	55	2.701	0.49
1469	29335	B7V	65	2.75	0.51
1484	29589	B8IV	70	2.728	0.45
1576	31373	B9V	70	2.731	0.52
1600	31764	B7V	140	2.71	0.68
1610	32040	B9Vn	295	2.77	0.69
1671	33224	B8V	155	2.755	0.64
1696	33802	B8V	185	2.755	0.59
1705	33949	B7V	120	2.717	0.70
1750	34762	B9IV	230	2.743	0.72
1757	34863	B7/B8V	285	2.734	0.62
1759	34880	B8III	45	2.724	0.59
1769	35104	B8II	95	2.725	0.47
1791	35497	B7III	60	2.703	0.56
1860	36589	B6V	90	2.728	0.52
1902	37098	B9IV-V	50	2.768	0.58
1920	37320	B8III	25	2.736	0.64
1945	37646	B8IV	130	2.762	0.60
1957	37808	B9.5IIIsp	30	2.722	0.45
1985	38478	B8IIImnp	55	2.705	0.58
1997	38670	B9Vn	215	2.745	0.59
2038	39417	B9V	145	2.75	0.66

Table 2—Continued

HR	HD	Sp. Type	*v sin i* (km s^{-1})	β	c_0
2109	40574	B8IIIn	205	2.709	0.64
2116	40724	B8V	130	2.776	0.73
2127	40964	B8V	115	2.782	0.72
2130	41040	B8III	140	2.718	0.60
2139	41269	B9sp	85	2.766	0.71
2202	42657	B9mnp	65	2.737	0.55
2207	42784	B8Vnn	370	2.72	0.57
2223	43153	B7V	65	2.756	0.57
2237	43362	B9III	145	2.77	0.71
2248	43526	B7III	75	2.696	0.52
2297	44766	B8IIIn	170	2.745	0.60
2374	46075	B6III	50	2.736	0.62
2438	47395	B7III	65	2.714	0.53
2454	47756	B8IIIs	30	2.715	0.58
2461	47964	B8III	45	2.718	0.72
2497	49028	B8IV	45	2.72	0.49
2519	49606	B7III	20	2.702	0.50
2521	49643	B8IIIn	255	2.723	0.52
2522	49662	B7IV	90	2.751	0.45
2589	51104	B8Vn	160	2.753	0.67
2605	51688	B8III	35	2.705	0.53
2613	51892	B7III	50	2.704	0.56
2676	53929	B9.5III	25	2.708	0.53
2760	56446	B8III	185	2.725	0.65
2826	58346	B8/B9V	165	2.754	0.72
2860	59136	B5III	65	2.712	0.64
2922	60863	B8V	185	2.756	0.59
2947	61554	B6V	280	2.712	0.52
2949	61556	B5IVn	70	2.75	0.57
2956	61672	B7V	280	2.726	0.59
3201	68099	B6III	50	2.72	0.62
3353	71997	B4V	15	2.72	0.47
3470	74604	B8V	150	2.759	0.61
3500	75333	B9mnp	35	2.747	0.63
3607	77665	B8V	90	2.738	0.72
3652	79158	B8IIImnp	60	2.706	0.55
3982	87901	B7V	300	2.723	0.71
4119	90994	B6V	80	2.73	0.48
4493	101391	B9p	50	2.765	0.59
4696	107348	B8V	195	2.738	0.71
4857	111226	B8V	70	2.73	0.60
4967	114376	B7III	115	2.712	0.52
5250	121847	B8V	165	2.757	0.66
5407	126769	B8V	195	2.753	0.57
5475	129174	B9p	25	2.745	0.54

Table 2—Continued

HR	HD	Sp. Type	*v sin i* (km s^{-1})	β	c_0
5597	133029	B9sp	30	2.8	0.69
5614	133529	B7V	310	2.732	0.57
5655	134946	B8III	150	2.738	0.52
5733	137391	F0V	90	2.745	0.74
5780	138764	B6IV	20	2.72	0.50
5910	142250	B6Vp	15	2.75	0.49
6003	144844	B9V	20	2.791	0.58
6023	145389	B9mnp	20	2.787	0.69
6054	146001	B8V	90	2.748	0.49
6079	146926	B8V	180	2.736	0.70
6294	152909	B7/B8III	50	2.752	0.57
6340	154204	B7IV/V	275	2.725	0.51
6520	158704	B9II/III	20	2.757	0.57
6545	159376	Ap	164	2.726	0.68
6567	159975	B8II-IIImnp	95	2.718	0.74
6720	164447	B8Vne	170	2.721	0.65
6919	169990	B8III/IV	110	2.764	0.71
6967	171247	B8IIIsp	55	2.717	0.73
6968	171301	B8IV	40	2.772	0.69
6990	171961	B8III	55	2.721	0.54
6997	172044	B8II-IIIp	30	2.696	0.48
7035	173117	B8III	30	2.705	0.58
7039	173300	B8III	35	2.733	0.71
7073	173936	B6V	90	2.739	0.47
7113	174933	B9II-IIIp	20	2.753	0.58
7115	174959	B6IV	50	2.707	0.49
7147	175744	B9sp	50	2.701	0.49
7239	177817	B7V	130	2.742	0.68
7241	177863	B8V	60	2.731	0.57
7245	178065	B9III	15	2.718	0.71
7248	178125	B8III	60	2.755	0.59
7283	179527	B9sp	35	2.712	0.67
7285	179588	B9IV	35	2.812	0.69
7339	181558	B5III	20	2.715	0.44
7346	181828	B9V	145	2.747	0.61
7358	182255	B6III	25	2.736	0.48
7361	182308	B9mnp	15	2.699	0.47
7395	183056	B9sp	35	2.714	0.52
7401	183339	B8IVwe	45	2.706	0.48
7437	184606	B8IIIn	185	2.709	0.64
7447	184930	B5III	55	2.707	0.56
7452	184961	B9sp	40	2.789	0.70
7457	185037	B8Vne	315	2.717	0.73
7466	185268	B5V	195	2.694	0.46
7493	186122	B9III	20	2.729	0.63

Table 2—Continued

HR	HD	Sp. Type	*v sin i* (km s^{-1})	β	c_0
7543	187235	B8Vn	315	2.76	0.68
7593	188293	B7Vn	190	2.73	0.51
7607	188651	B6V+	150	2.715	0.52
7608	188665	B5V	105	2.715	0.45
7642	189432	B5IV	15	2.723	0.48
7664	190229	B9mnp	20	2.695	0.51
7721	192276	B7V	25	2.745	0.54
7737	192659	B9IV-V	20	2.769	0.62
7786	193722	B9sp	35	2.711	0.63
7814	194636	B4V	30	2.763	0.60
7840	195483	B8V	140	2.759	0.53
7852	195810	B6III	50	2.702	0.55
7878	196426	B8IIIp	20	2.735	0.62
7885	196606	B8IIIn	50	2.729	0.62
7922	197226	B6III	90	2.736	0.54
7961	198174	B7IIIp	65	2.705	0.59
7963	198183	B5Ve	100	2.71	0.51
7978	198513	B8np	175	2.761	0.70
8022	199578	B5V	30	2.71	0.46
8033	199728	Ap	55	2.732	0.63
8065	200614	B8III	20	2.714	0.74
8094	201433	B9V	25	2.789	0.71
8106	201834	B9III	25	2.732	0.57
8109	201888	B7III	5	2.725	0.53
8118	202149	B9mnp	35	2.78	0.71
8141	202753	B5V	20	2.703	0.48
8158	203206	B6IV	60	2.755	0.52
8161	203245	B6V	75	2.731	0.50
8218	204428	B6V	125	2.726	0.53
8226	204754	B8III	20	2.709	0.66
8240	205087	B9sp	30	2.799	0.66
8292	206540	B5IV	20	2.719	0.50
8338	207516	B8V	95	2.784	0.71
8348	207840	B8III	15	2.755	0.62
8349	207857	B9mnp	20	2.704	0.50
8355	208008	B9V	45	2.743	0.50
8377	208727	B8V	205	2.758	0.61
8403	209419	B5III	20	2.697	0.48
8418	209819	B8V	135	2.793	0.70
8452	210424	B5III	20	2.723	0.53
8478	210934	B8III	50	2.736	0.66
8512	211838	B8IIImnp	65	2.721	0.68
8554	212986	B5III	30	2.736	0.49
8705	216523	B8V	30	2.761	0.59
8706	216538	B7III-IV	20	2.706	0.55

Table 2—Continued

HR	HD	Sp. Type	*v sin i* (km s^{-1})	β	c_0
8723	216831	B7III	65	2.714	0.62
8861	219749	B9p	65	2.765	0.66
8873	219927	B8III	15	2.718	0.64
8887	220222	B6III	115	2.708	0.56
8902	220575	B8III	20	2.717	0.74
9031	223640	Ap	30	2.751	0.56
9086	224906	B9IIImnp	35	2.725	0.68
9087	224926	B7III-IV	60	2.703	0.50
9091	224990	B4III	15	2.706	0.46
9110	225289	B8mnp	40	2.719	0.63
Group 2					
38	829	B2V	0	2.652	0.20
91	1976	B5IV	125	2.693	0.38
155	3379	B2.5IV	55	2.695	0.26
189	4142	B5V	160	2.702	0.41
302	6300	B3V	100	2.68	0.33
801	16908	B3V	90	2.682	0.32
930	19268	B5V	25	2.719	0.43
950	19736	B4V	50	2.677	0.36
987	20365	B3V	120	2.681	0.34
989	20418	B5V	260	2.673	0.39
1005	20756	B5IV	30	2.718	0.37
1011	20809	B5V	185	2.696	0.39
1029	21071	B7V	50	2.727	0.44
1034	21278	B5V	50	2.705	0.40
1044	21428	B3V	125	2.686	0.36
1063	21699	B8IIImnp	35	2.696	0.37
1121	22920	B9IIIsp	30	2.687	0.43
1153	23466	B3V	90	2.688	0.31
1174	23793	B3V	20	2.684	0.34
1194	24155	B9sp	35	2.706	0.34
1199	24263	B5V	105	2.711	0.44
1244	25340	B5V	80	2.708	0.43
1253	25558	B3V	30	2.694	0.32
1258	25631	B2.5V	220	2.654	0.18
1312	26739	B5IV	30	2.677	0.40
1350	27396	B4IV	15	2.678	0.36
1378	27778	B3V	105	2.682	0.34
1415	28355	B3V	0	2.713	0.40
1553	30870	B5V	110	2.701	0.37
1582	31512	B6V	80	2.695	0.43
1617	32249	B3V	30	2.656	0.23
1640	32612	B2.5IV	65	2.665	0.18
1641	32630	B3V	95	2.684	0.31

Table 2—Continued

HR	HD	Sp. Type	*v sin i* (km s^{-1})	β	c_0
1719	34233	B5V	35	2.71	0.42
1731	34447	B3IV	10	2.657	0.24
1748	34748	B1.5Vn	295	2.639	0.14
1749	34759	B3V	55	2.717	0.38
1753	34798	B5IV/V	30	2.703	0.37
1765	35039	B2IV-V	5	2.628	0.16
1786	35407	B4IVn	295	2.683	0.32
1798	35532	B2Vn	260	2.623	0.24
1810	35708	B2.5IV	10	2.642	0.14
1820	35912	B2V	5	2.671	0.20
1839	36267	B5V	155	2.724	0.41
1848	36430	B2V	15	2.674	0.19
1851	36485	B2V	35	2.653	0.17
1864	36653	B3V	155	2.685	0.31
1871	36741	B2V	175	2.65	0.15
1875	36819	B2.5IV	105	2.671	0.26
1891	37016	B2.5V	100	2.687	0.25
1898	37040	B2.5IV	145	2.68	0.24
1900	37055	B3IV	50	2.716	0.30
1906	37150	B3Vvar	190	2.653	0.14
1924	37367	B2IV-V	20	2.629	0.19
1928	37438	B3IV	40	2.668	0.25
1946	37711	B3IV	105	2.672	0.31
1951	37752	B8p	35	2.697	0.40
2005	38804	B5V	40	2.713	0.43
2128	40967	B5III	45	2.679	0.35
2161	41814	B3V	35	2.718	0.28
2198	42545	B5Vn	245	2.68	0.40
2199	42560	B3IV	160	2.669	0.33
2205	42690	B2V	0	2.634	0.20
2213	42927	B3III	95	2.682	0.26
2224	43157	B5V	30	2.673	0.29
2232	43317	B3IV	130	2.665	0.30
2266	43955	B2/B3V	40	2.661	0.24
2273	44112	B2.5V	95	2.65	0.22
2282	44402	B2.5V	25	2.677	0.26
2292	44700	B3V	0	2.696	0.33
2306	44953	B8III	30	2.691	0.31
2325	45321	B2.5V	160	2.684	0.31
2344	45546	B2V	70	2.652	0.20
2361	45813	B4V	120	2.692	0.37
2380	46189	B2.5V	85	2.673	0.30
2433	47247	B3V	70	2.72	0.39
2490	48879	B4IV	105	2.668	0.35
2494	48977	B2.5V	20	2.669	0.25

Table 2—Continued

HR	HD	Sp. Type	*v sin i* (km s^{-1})	β	c_0
2509	49333	B7II/III	65	2.689	0.32
2537	50012	B2IV	70	2.62	0.16
2544	50093	B2III/IV	150	2.632	0.21
2603	51630	B2III/IV	20	2.616	0.15
2611	51823	B2.5V	70	2.676	0.29
2614	51925	B2.5III	165	2.636	0.15
2616	52018	B2V	50	2.666	0.25
2621	52140	B3V	0	2.702	0.35
2623	52273	B2III	80	2.605	0.16
2625	52348	B3V	145	2.677	0.31
2640	52670	B2V	17	2.635	0.28
2680	54031	B3V	0	2.689	0.32
2688	54224	B2IV-V	10	2.645	0.19
2695	54669	B4V	115	2.645	0.15
2704	54912	B2.5IV	40	2.639	0.19
2718	55522	B2IV/V	95	2.664	0.26
2756	56342	B3V	5	2.676	0.34
2774	56876	B2IV-V	310	2.676	0.37
2799	57573	B2.5V	190	2.667	0.33
2800	57593	B2.5V	105	2.659	0.25
2824	58325	B2IV-V	5	2.645	0.17
2921	60855	B2/B3V	240	2.609	0.18
2948	61555	B6V	107	2.714	0.28
3192	67797	B5IV	140	2.684	0.39
3194	67880	B2.5V	15	2.63	0.20
3454	74280	B3V	95	2.653	0.24
3849	83754	B5V	150	2.7	0.40
4456	100600	B4V	140	2.688	0.32
5191	120315	B3V	150	2.694	0.30
5764	138485	B2Vn	210	2.654	0.17
5902	142096	B2.5V	155	2.703	0.25
5904	142114	B2.5Vn	250	2.68	0.22
5907	142184	B2V	280	2.662	0.25
5912	142301	B8III/IV	90	2.693	0.29
5915	142378	B2/B3V	225	2.69	0.32
5928	142669	B2IV-V	120	2.647	0.15
5942	142990	B5IV	125	2.682	0.24
5985	144218	B2V	65	2.675	0.14
5988	144334	B8V	55	2.721	0.34
5998	144661	B8IV/V	45	2.708	0.39
6042	145792	B6IV	30	2.725	0.39
6092	147394	B5IV	30	2.702	0.44
6141	148605	B2V	175	2.662	0.18
6502	158148	B5V	240	2.688	0.43
6588	160762	B3IV	0	2.661	0.29

Table 2—Continued

HR	HD	Sp. Type	*v sin i* (km s^{-1})	β	c_0
6692	163685	B3IV	10	2.679	0.37
6741	164900	B3Vn	260	2.67	0.32
6851	168199	B5V	175	2.687	0.39
6873	168797	B3Ve	260	2.644	0.24
6924	170111	B3V	120	2.692	0.34
6946	170740	B2V	25	2.641	0.15
6984	171780	B5Vne	230	2.688	0.42
7033	173087	B5V	85	2.712	0.37
7081	174179	B3IVpsh	5	2.657	0.29
7100	174585	B3IV	145	2.66	0.25
7121	175191	B2.5V	165	2.667	0.21
7166	176162	B5IV	200	2.703	0.35
7179	176502	B3V	0	2.667	0.32
7185	176582	B5IV	65	2.692	0.26
7210	177003	B2.5IV	10	2.675	0.24
7258	178329	B3V	0	2.69	0.32
7306	180554	B4IV	80	2.677	0.39
7347	181858	B3IVp	0	2.696	0.34
7355	182180	B2Vn	320	2.666	0.23
7372	182568	B3IV	100	2.667	0.22
7374	182618	B5V	35	2.706	0.41
7467	185330	B5II-III	15	2.667	0.37
7565	187811	B2.5Ve	195	2.667	0.28
7647	189687	B3IVe	230	2.638	0.28
7651	189775	B5III	85	2.668	0.32
7656	189944	B4V	10	2.704	0.44
7700	191263	B3V	60	2.68	0.30
7739	192685	B3V	160	2.658	0.27
7862	196035	B3IV	20	2.688	0.28
7870	196178	B9sp	50	2.709	0.38
7899	196775	B3V	210	2.665	0.25
7911	197018	B6IIImnp	55	2.699	0.44
7912	197036	B5IV	135	2.679	0.35
7927	197419	B2IV-Ve	105	2.655	0.28
7929	197511	B2V	35	2.651	0.30
7996	198820	B3III	15	2.677	0.38
8029	199661	B2.5IV	130	2.682	0.28
8064	200595	B3Vn	285	2.682	0.42
8136	202654	B4IV	160	2.68	0.29
8301	206672	B3IV	55	2.642	0.29
8341	207563	B2V	85	2.647	0.25
8356	208057	B3Ve	110	2.673	0.31
8439	210191	B2.5IV	10	2.627	0.23
8520	212076	B2IV-Ve	80	2.608	0.16
8528	212222	B5V	35	2.715	0.43

Table 2—Continued

HR	HD	Sp. Type	*v sin i* (km s^{-1})	β	c_0
8535	212454	B8III-IV	40	2.694	0.42
8549	212883	B2V	5	2.659	0.17
8553	212978	B2V	120	2.646	0.16
8579	213420	B2IV	70	2.625	0.17
8758	217543	B3Vpesh	305	2.662	0.23
8768	217811	B2V	0	2.661	0.25
8770	217833	B9IIIwe	30	2.691	0.37
8777	217943	B2V	145	2.664	0.18
9011	223229	B3IV	30	2.68	0.29
Group 3					
39	886	B2IV	0	2.629	0.12
153	3360	B2IV	10	2.625	0.13
779	16582	B2IV	5	2.624	0.10
1072	21803	B2IV	40	2.61	0.06
1191	24131	B1V	95	2.623	0.01
1215	24640	B1.5V	150	2.646	0.09
1463	29248	B2III	20	2.612	0.07
1552	30836	B2III+	35	2.606	0.13
1595	31726	B1V	5	2.634	0.05
1679	33328	B2IVne	325	2.604	0.05
1770	35149	B1V	220	2.617	0.05
1781	35299	B1.5V	0	2.636	0.05
1783	35337	B2IV	15	2.632	0.06
1790	35468	B2III	55	2.613	0.11
1833	36166	B2V	125	2.641	0.10
1840	36285	B2IV-V	15	2.646	0.11
1842	36351	B1.5V	20	2.639	0.11
1855	36512	B0V	10	2.597	0.09
1861	36591	B1IV	5	2.61	-0.01
1873	36779	B2.5V	175	2.649	0.13
1886	36959	B1Vvar	5	2.629	0.04
1887	36960	B0.5V	20	2.6	0.05
1892	37018	B1V	20	2.619	-0.01
1896	37023	B0.5Vp	80	2.61	0.00
1911	37209	B1V	35	2.63	0.04
1913	37232	B2IV-V	110	2.642	0.08
1918	37303	B1Vvar	265	2.618	0.01
1923	37356	B2IV-V	10	2.623	0.10
1932	37479	B2VpHe	165	2.586	0.03
1933	37481	B1.5IV	90	2.636	0.06
1950	37744	B1.5V	25	2.634	0.04
2031	39291	B2IV-V	150	2.639	0.10
2058	39777	B1.5V	20	2.65	0.11
2294	44743	B1II/III	17	2.593	0.00

Table 2—Continued

HR	HD	Sp. Type	*v sin i* (km s^{-1})	β	c_0
2373	46064	B2III	60	2.638	0.14
2387	46328	B1III	0	2.585	0.02
2618	52089	B2Iab:	25	2.577	0.00
2628	52437	B3Vnn	190	2.622	0.14
2648	52918	B1V	270	2.591	0.01
2733	55856	B2IV	40	2.614	0.10
2734	55857	B0.5V	150	2.605	0.07
2739	55879	B0III	30	2.588	0.09
2743	55985	B2IV-V	30	2.632	0.13
2928	61068	B2III	10	2.62	0.05
3004	62747	B1.5III	95	2.6	0.06
3023	63271	B2IV-V	30	2.643	0.08
5885	141637	B1.5Vn	225	2.637	0.10
6453	157056	B2IV	30	2.623	0.10
6601	161056	B1.5V	235	2.594	0.05
6684	163472	B2IV-V	75	2.63	0.10
6719	164432	B2IV	50	2.614	0.13
6787	166182	B2IV	30	2.608	0.15
7335	181409	B2IVe	140	2.615	0.02
7940	197770	B2III	55	2.596	0.12
8007	199140	B2III	45	2.611	0.02
8238	205021	B1IV	20	2.628	0.01
8603	214167	B2Ve	265	2.609	0.01
8640	214993	B2III	30	2.612	0.04
8651	215191	B1V	180	2.633	0.06
8725	216916	B2IV	10	2.639	0.08
8733	217101	B2IV-V	130	2.663	0.10
9005	223128	B2IV	10	2.634	0.08
9071	224572	B1V	150	2.608	0.06

Table 3. Data for Field Star Binaries

HR	HD	Sp. Type	*v sin i* (km s^{-1})	β	c_0	K (km s^{-1})
Group 1						
354	7157	B9V	22	2.789	0.632	abt:sb2
936	19356	B8V	50	2.748	0.616	sb2:44
1033	21203	B9V+...	50	2.791	0.684	abt:sb2
1088	22203	B9V	65	2.765	0.702	sb2:103
1185	23950	B8III	60	2.746	0.607	abt:sb2
1240	25267	B6V+...	30	2.733	0.611	sb1:41
1347	27376	B9V	20	2.768	0.63	sb2:64
1471	29365	B8V	70	2.757	0.601	sb1:65
1690	33647	B9Vn	30	2.771	0.687	abt:sb2
1847	36408	B7IIIe	45	2.711	0.706	abt:sb2
2226	43179	B7V	25	2.763	0.616	abt:sb2
2784	57103	B8V	55	2.774	0.648	sb2:106
3623	78316	B8IIImnp	15	2.717	0.558	sb1:67
5801	139160	B7IV	25	2.74	0.451	sb1:37
5863	140873	B8III	80	2.744	0.499	sb2:43
5906	142165	B5V	220	2.74	0.481	sb1:33
6620	161701	B9V	25	2.754	0.641	sb1:52
6928	170200	B8III-IV	40	2.745	0.631	sb1:38
7109	174853	B8Vnn	100	2.763	0.636	abt:sb2
7171	176301	B7III-IV	75	2.707	0.593	abt:sb2
7174	176318	B7IV	120	2.75	0.579	sb1:76
7326	181182	B8III+	60	2.725	0.603	sb2:70
8036	199892	B7III	20	2.731	0.535	sb1:43
8357	208095	B6IV-V	95	2.747	0.508	sb2:106
8567	213236	B8II	15	2.737	0.669	abt:sb2
Group 2						
154	3369	B5V	25	2.688	0.433	sb2:48
226	4727	B5V	20	2.71	0.407	sb2:72
1163	23625	B2.5V	20	2.654	0.146	sb2:82
1239	25204	B3V+...	50	2.691	0.352	sb2:57
1288	26326	B4V	5	2.69	0.391	abt:sb2
1420	28475	B5V	30	2.711	0.432	sb2:80
1497	29763	B3V	115	2.713	0.356	sb2:54
1659	32990	B2V	55	2.64	0.241	sb1:37
1764	35007	B3V	35	2.691	0.277	abt:sb2
1803	35588	B2.5V	170	2.663	0.189	sb1:71
1863	36646	B4Vn	180	2.69	0.271	abt:sb2
1890	37017	B1.5V	165	2.65	0.136	sb1:36
2052	39698	B2V	115	2.635	0.185	sb2:70
2159	41753	B3V	30	2.653	0.317	sb1:33
2598	51411	B3V	0	2.707	0.376	abt:sb2
5812	139365	B2.5V	100	2.689	0.263	sb2:75
5934	142883	B3V	5	2.721	0.317	sb1:64

Table 3—Continued

HR	HD	Sp. Type	*v sin i* (km s^{-1})	β	c_0	K (km s^{-1})
6028	145482	B2V	165	2.657	0.177	sb1:32
6414	156247	B5Vnn	110	2.695	0.390	sb2:180
6431	156633	B1.5V	140	2.648	0.206	sb2:98
6621	161756	B4IVe	95	2.665	0.349	abt:sb2
6738	164852	B3IV	150	2.685	0.295	sb2:58
6773	165814	B4IV	200	2.674	0.389	sb2:151
7131	175426	B2.5V	110	2.666	0.303	sb1:40
7305	180553	B8V	70	2.704	0.362	sb1:55
7486	185936	B5V	65	2.704	0.426	sb1:47
7688	190993	B3V	115	2.686	0.293	abt:sb2
7777	193536	B2V	80	2.63	0.219	sb2:115
7861	195986	B4III	0	2.672	0.385	sb1:32
8001	199081	B5V	40	2.713	0.397	sb2:112
8384	208947	B2V	125	2.654	0.188	sb2:116
8397	209288	B5IIIn	75	2.7	0.390	abt:sb2
8427	209961	B2V	145	2.638	0.167	sb1:122
8606	214240	B3V	55	2.678	0.374	sb1:82
8800	218407	B2V	100	2.639	0.165	sb1:86
8803	218440	B2V	25	2.664	0.166	sb2:88
8808	218537	B3V	80	2.695	0.255	abt:sb2
8926	221253	B3IV	140	2.681	0.295	sb1:57
Group 3						
1131	23180	—	100	2.597	0.022	sb2;112
1333	27192	B1.5IV	110	2.604	0.027	abt:sb2
1567	31237	B3III+	90	2.603	0.135	sb1:58
1811	35715	B2IV	110	2.622	0.027	sb2:139
1868	36695	B1V	120	2.625	0.012	sb2;129
1894	37021	B0V	240	2.602	0.125	sb2:66
1952	37756	B2IV-V	75	2.632	0.111	sb2:89
4590	104337	B1.5V	95	2.607	0.078	sb2:120
5056	116658	B1III-IV	130	2.607	0.018	sb2:120
5944	143018	B1V	90	2.614	0.016	sb2:124
5984	144217	B1V	100	2.615	-0.017	sb2:125
7200	176819	B2IV-V	40	2.640	0.095	sb1:55

Table 4. Average Values of $v \sin i$

Definition of Sample	$\langle v \sin i \rangle$ (km s^{-1})	No. of Stars
Group 1		
All Stars		
h and χ Per Members	183	72
Field Stars	92	259
Binaries K > 30 km s^{-1} excluded		
h and χ Per Members	184	62
Field Stars	96	234
Binaries K > 30 km s^{-1} only		
h and χ Per Members	183	10
Field Stars	56	25
Group 2		
All Stars		
h and χ Per Members	145	82
Field Stars	93	215
Binaries K > 30 km s^{-1} excluded		
h and χ Per Members	156	73
Field Stars	95	177
Binaries K > 30 km s^{-1} only		
h and χ Per Members	44	9
Field Stars	84	38
Group3		
All Stars		
h and χ Per Members	104	45
Field Stars	83	75
Binaries K> 30 km s^{-1} excluded		
h and χ Per Members	104	42
Field Stars	79	63
Binaries K > 30 km s^{-1} only		
h and χ Per Members	100	3
Field Stars	108	12

Table 5. Binary Frequency: K > 30 km s^{-1}

Definition of Sample	Total No. of Stars	No. of Binaries	Binary Fraction
Group 1			
Field	259	25	0.1
Binary Fraction Detected in Single Observation			0.06
h and χ Per Detected Binaries	71	9	0.13
Group 2			
Field Stars	215	38	0.18
Binary Fraction Detected in Single Observation			0.12
h and χ Per Detected Binaries	79	6	0.08
Group 3			
Field Stars	75	12	0.16
Binary Fraction Detected in Single Observation			0.13
h and χ Per Detected Binaries	45	3	0.07
Total Sample			
Field Stars	549	75	0.14
Binary Fraction Detected in Single Observation			0.09
h and χ Per Detected Binaries	195	18	0.09